Virtual Screening Identifies Irreversible FMS-like Tyrosine Kinase 3 Inhibitors with Activity towards Resistance-conferring Mutations

*Dennis Bensinger[†], Daniel Stubba[†], Anjali Cremer[‡], Vanessa Kohl[†], Theresa Waßmer[†], Johanna Stuckert[†], Victoria Engemann[†], Kimberly Stegmaier[‡], Katja Schmitz[†] and Boris Schmidt[†]**

[†]Clemens-Schöpf-Institute for Organic Chemistry and Biochemistry, Technische Universität Darmstadt, 64287 Darmstadt, Germany

[‡]Department of Pediatric Oncology, Dana-Farber Cancer Institute, Harvard Medical School, Boston, Massachusetts 02215, United States

Abstract

The use of covalent irreversible binding inhibitors is an established concept for drug development. Usually the discovery of new irreversible kinase inhibitors occurs serendipitously showing that efficient rational approaches for the rapid discovery of new drugs are needed. Herein, we report a virtual screening strategy that led to the discovery of irreversible inhibitors of the FMS-like tyrosine kinase 3 (FLT3) involved in the pathogenesis of acute myeloid leukemia (AML). A virtual screening library was designed to target the highly conserved Cys828 residue preceding the DFG motif by modification of reported reversible inhibitors with chemically reactive groups. Prospective covalent docking allowed the identification of two lead series, resulting in a massive increase in inhibition of kinase activity and cell viability by irreversible inhibitors compared to the corresponding reversible scaffolds. Lead compound 4b (BSc5371) displays superior cytotoxicity in FLT3-dependent cell lines to compounds in recent clinical trials and overcomes drug-resistant mutations.

Introduction

Acute myeloid leukemia (AML) is a malignant neoplasia affecting hematopoietic progenitor cells. These cells fail to differentiate into functional blood cells of the myeloid path (erythrocytes, neutrophils and thrombocytes), while ongoing cell proliferation leads to the accumulation of myeloblasts in the bone marrow.[1] The most common pathogenic mutations occur on the gene encoding for FMS-like tyrosine kinase 3 (FLT3). Length mutations in this gene through internal tandem duplications (ITD) in the juxtamembrane domain occur in about 25% of patients and lead to ligand-independent auto-phosphorylation and downstream signaling.[2] Point mutations in the FLT3 kinase domain (e.g. D835Y) occur in 10% of patients and destabilize the inactive kinase conformation leading to higher kinase activity.[3] In 2017 the multitargeted kinase inhibitor Midostaurin (PKC412) was approved by the US Food and Drug Administration (FDA) in combination with chemotherapy for the treatment of de novo FLT3-mutated AML showing a 22% reduction of risk of death.[4] Minimal residual disease after treatment with tyrosine kinase inhibitors (TKIs) like sorafenib and quizartinib can lead to relapse and is often associated with resistance-conferring point mutations in an FLT3-ITD allele.[2] As emergence of drug-resistant mutations is a common liability of targeted therapies, new agents with distinct properties are needed. The use of irreversibly binding TKIs has several advantages over classical reversible inhibitors such as an increased target residence time, altered selectivity, as well as more durable responses than their reversibly binding counterparts while idiosyncratic toxicity and sustained off-target effects are additional risks.[5] They act by the formation of a covalent bond between an amino acid with a nucleophilic side chain such as cysteine and a chemically reactive electrophilic group (CRG) connected to a specific ligand. Bond formation usually takes place after a strong non-covalent complex has formed that positions the CRG in

close vicinity to the target nucleophile. Upon covalent bond formation, irreversible reactions rule out ligand dissociation leading to non-equilibrium inhibition kinetics. Thus, the enzyme function can be restored by *de novo* synthesis only.

So long, four TKIs are approved by the FDA for the treatment of certain malignancies, afatinib,[6] neratinib,[7] osimertinib,[8] and ibrutinib,[9] act by irreversibly inhibiting the EGF-receptor family and Bruton´s tyrosine kinase, respectively.

The natural product hypothemycin is a resorcylic acid lactone that irreversibly inhibits 18 kinases, including FLT3.[10] The cis-enone motif is attacked by a cysteine directly preceding the DFG motif at the start of the activation loop (Cys828 in FLT3). These so-called "group 4" cysteines are the most conserved in the human kinome occurring in 48 of about 500 kinases.[11] A crystal structure analysis of hypothemycin and ERK2 confirms covalent binding in the DFG-in conformation.[12] Despite the advantages of irreversible inhibitors, only few drug development efforts have focused on targeting this group of cysteines. Examples include benzoquinone-substituted quinazolines targeting VEGFR2[13] and analogues or ring-opened derivatives of resorcylic acid lactones targeting FLT3, showing only micromolar cellular activity.[14]

Recently, discovery of covalent binding inhibitors was advanced by the development of molecular modelling algorithms that allow covalent docking.[15] In 2015, our group introduced the covalent docking tool DOCKTITE[16] as a freely available script package for the Molecular Operating Environment.[17] In this method a CRG is tagged by a pre- or user-defined trans-formation, that is then attached to a selected covalent attachment point of the receptor. During docking the nucleophilic residue is detached from the receptor but fixed by a tight pharmacophore. This strategy allows highly customizable virtual screening strategies while all

docking steps can be monitored and controlled. Consequently, DOCKTITE has been successfully used for the development of covalent inhibitors for the cysteine proteases rhodesain,[18-19] cruzain[18] and falcipain[20] as well as for the plasmodium proteasome.[21] Despite the recent progress described, only one case study identifying covalent kinase inhibitors in silico has been reported so far. London et al. successfully used the DOCKovalent tool to identify covalent reversible inhibitors of the kinases RSK2 and JAK3[22] as well as irreversible MKK7 inhibitors, that were published while this study was under revision.[23] However, the scope of covalent docking methodology has to be enlarged, as only cyano acrylamides and acrylamides were evaluated and hit identification profited by available protein-ligand structures with the modified target cysteine (RSK2) or numerous cocrystal structures with related hinge binders (JAK3, MKK7), respectively.

Because of the impressive clinical benefits of irreversible inhibitors and the vulnerability of FLT3 treatment to resistance we sought to rationally design and evaluate irreversible FLT3 inhibitors.

In the following, we present a strategy that allows the identification of irreversible FLT3 inhibitors with superior cytotoxicity to inhibitors in clinical trials that can overcome resistance-conferring mutations of FLT3.

Results and Discussion

Rational Design of Irreversible FLT3 Inhibitors. A major drawback of FLT3 inhibitors in recent clinical trials was the acquisition of point mutations within the ATP-binding site thus we decided to target FLT3 in its catalytically active DFG-in conformation. Within the ATP-binding site FLT3 possesses three targetable cysteine residues. Two of them, Cys694 (gatekeeper + 3)

and Cys695 (gatekeeper + 4), are part of the hinge region while Cys828 is preceding the conserved DFG-motif. Kinase inhibitors usually gain potency by forming alternating hydrogen bond donor/acceptor interactions with the hinge backbone atoms. Therefore modification of known hinge binding motifs are promising starting points to target the neighboring Cys828 residue. Additionally, exposure of Cys828 to the surface of the ATP binding pocket allows variation of the trajectory by which a CRG is recognized and a covalent bond can be formed. However, no crystal structure of FLT3 in the active conformation has been reported, so we designed a homology model of the active FLT3 conformation using c-KIT (pdb 1PKG) as a template (Figure S1-S3).[24]

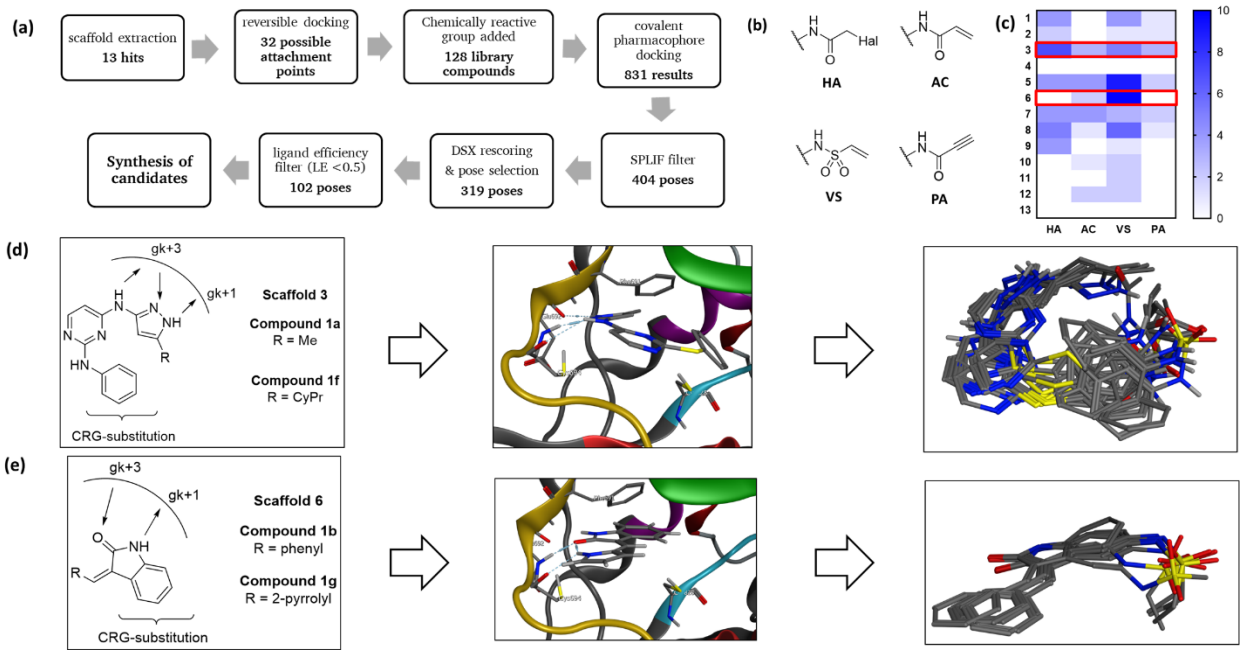

Figure 1. (a) Virtual screening and filter strategy for the *in silico* discovery of irreversible FLT3 inhibitors; (b, c) Structure of CRGs and pose distribution among scaffolds. HA: α-halo acetamide, AC: acrylamide, VS: vinyl sulfonamide and PA: propargyl amide (d) Rational design

and docking hits of the bisaminopyrimidine scaffold 3 and (e) the indolinone inhibitor scaffold 6 (gk = gatekeeper residue).

c-KIT is the most closely related kinase to FLT3 with a sequence similarity of 79% and a sequence identity of 64% and consequently numerous shared potent inhibitors.[25] To validate the homology model, we docked hypothemycin covalently to Cys828 of FLT3. Rigid body alignment of the top-scored conformation docked into FLT3 with the conformation obtained from the co-crystallized structure in ERK2 gave a r.m.s. deviation (RMSD) of 1.34 Å, while the top-scored redocked pose in ERK2 showed a RMSD of 1.08 Å (Figure S4). To identify potent reversible inhibitors as starting points for reactive modifications and subsequent covalent docking, the publicly accessible BindingDB Database was manually searched for FLT3 inhibitors with distinct hinge binding motifs (Figure 1a, 1752 entries as of Jan. 2015).[26] Typical inhibitors that were excluded contain bisarylurea motifs such as sorafenib, quizartinib and ponatinib that are designed to occupy the hydrophobic pocket II and thus bind to the inactive DFG-out conformation.[2] We found a set of 13 different hinge binding scaffolds (Figure S5) and identified a plausible reversible binding pose for each scaffold (Figure S6 – S18). Those scaffolds form mono- (5 scaffolds), bi- (6 scaffolds) or tridentate (2 scaffolds) alternating hydrogen bond donor/acceptor interactions to the gatekeeper+1 (Glu692) and +3 residue (Cys694) that are comparable to hinge binding observed from crystal structures of related scaffolds.[27] We selected four chemically and sterically distinct CRGs (Figure 1b) to be attached to the non-covalent docked structure. The acrylamide (AC), vinyl sulfonamide (VS) and propargyl amide (PA) groups span approximately 5 Å, while the α-halo acetamide (HA) warhead spans only 3.8 Å (Figure S19). We concluded, that CRG-substitution of aromatic ring carbons

within 5 Å to the Cys828 sulfur may enable covalent binding (Figure S6F to S18F), while favorable conformations were selected by covalent docking. Subsequently, we identified 32 attachment points among the selected scaffolds leading to a targeted virtual library of 128 compounds (Table S1). Since addition of nucleophiles to the propargyl amide can lead to E- or Z- substituted alkenes, addition to the covalent attachment point prior to pharmacophore docking gave 160 docking input structures.

Virtual Screening and Filter Strategy. Covalent docking was performed using the pharmacophore placement method. The pharmacophore features of the 13 scaffolds were defined by the aryl, donor and acceptor groups forming hinge interactions and complemented with a tight pharmacophore at the target cysteine (Figure S6E to S18E). However, the pharmacophore feature of the nucleophilic sulfur atom in Cys828 was less stringent (d = 3.0 Å) allowing different rotamers. The initial docking gave 831 poses (Table S2, Figure S20) that were filtered for Glu692 and Cys694 backbone hydrogen bond donor acceptor interactions (404 poses left) and subsequently rescored using the DSX scoring function[28] while only the top 5 poses of every ligand were retained (319 poses left). We then calculated the ligand efficiency based on the London dG score and set a cutoff at -0.5 kcal/mol/heavy atom to limit the search to highly efficient inhibitors (102 poses left, Figure 1c, Table S3 – S5). From the reversible scaffolds, 5 scaffolds retain more than 10 hits of the corresponding reactive inhibitors (73% of total hits). On average, 32% of the initial docking hits in this group ranging from 13% (bisaminopyrimidine, scaffold 3) to 67% (indolinone, scaffold 6) are retained by the filter strategy. The hit distribution varies widely among the CRGs. With 45% of total hits vinyl sulfonamides are the most abundant group, followed by the α-halo acetamides (29%), acrylamides (16%) and propargyl amides (10%).

Characterization of Reversible Binding Fragments. As the potency of irreversible binding inhibitors is based on a moderate affinity between target and ligand in a reversible equilibrium prior to inactivation, we sought to evaluate the potency and structure-activity relationship of the selected reversible hits to further increase efficiency and the success rate of prospective irreversible inhibitor design. As the rational design starts from reported reversible ligands, synthetic procedures used to prepare reversible compounds **1a** to **1g** were based on earlier work (see experimental section). Among the initial series of reversible inhibitors (**1a** to **1e**), bisaminopyrimidine **1a** is the most cytotoxic compound (89% cell death, 10 μM, Table 1) and strongest inhibitor of FLT3wt. The indolinone **1b** shows a comparable inhibition for FLT3wt and FLT3(D835Y). Imidazopyridine **1c** and quinazoline **1d** are less potent inhibitors of FLT3(D835Y) while azaindole **1e** shows only weak inhibition of FLT3wt. However, all of the compounds of the initial series show only low cytotoxic activity in FLT3-ITD mutant MV4-11 cells. To increase reversible binding affinity, we applied small changes to the most promising inhibitors **1a** and **1b** that are compatible with the initial, reversible docking poses leaving the attachment points for the CRGs unchanged (Figure 1d, e; S21a, b). Exchange of the phenyl ring in **1b** with a 2-pyrrole (**1g**) constrains a planar conformation of the ligand by formation of an intramolecular hydrogen bond. The 5-methyl group connected to the pyrazolyl amine **1a** was changed to a cyclopropyl ring (**1f**) that has also been reported to efficiently target FLT3.[29] These small modifications massively increase the cytotoxicity of both scaffolds as well as inhibition of FLT3 and FLT3(D835Y) kinase activity making these fragments an efficient starting point for the development of irreversible inhibitors. The same modifications were applied to the poses obtained from the initial covalent docking and subsequent energy-minimization leaves the poses largely unchanged (Figure S21c – j).

Table 1. Inhibition of FLT3wt; FLT3(D835Y) and MV4-11 cell viability treated with reversible binding fragments. [a] Eurofins KinaseProfiler, [b] ADP-Glo Assay.

Structure	Compound	IC_{50} (MV4-11) / nM	Relative Inhibition (c_{TKI} = 1 µM) / %	
			FLT3wt [a]	FLT3 (D835Y)[b]
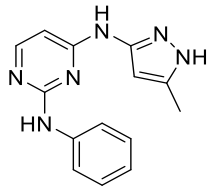	**1a**	> 1.000 nM	82	15
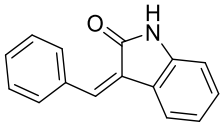	**1b**	> 1.000 nM	60	45
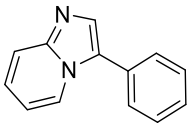	**1c**	> 1.000 nM	76	8
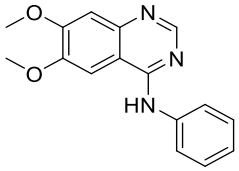	**1d**	> 1.000 nM	26	25
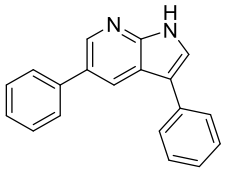	**1e**	> 1.000 nM	25	83
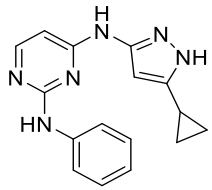	**1f**	230±53	98	88
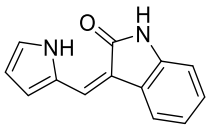	**1g**	380±21	97	86

Characterization of Indolinone-based Irreversible Inhibitors. A total of nine inhibitors based on the reversible indolinone hit **1g** were synthesized (Table 2). In addition to the CRG-substituted derivatives we synthesized the analogous unreactive inhibitors to assess the effect of the amide or sulfonamide linking group on reversible binding affinity. To evaluate the hit rate of the screening strategy, we also synthesized the inhibitors that were not identified as a hit during virtual screening. The 5-substituted vinyl sulfonamide **2i** was the most potent inhibitor of this series showing a 5-fold in-crease in inhibition of MV4-11 cell viability compared to the initial fragment as well as the highest inhibition of kinase activity in FLT3(D835Y) and FLT3(ITD) in this series. Importantly, the unreactive ethyl sulfonamide **2h** shows a massive decrease in inhibition of cell viability and kinase activity with decreased inhibition in FLT3(D835Y) and FLT3(ITD) suggesting that potency arises from covalent bond formation as both compounds are able to adopt the same reversible conformations. The vinyl sulfonamide warhead gave the highest number of hits *in silico* with the top virtual ligand-efficiency (LE_V) at rank 6 of the 102 hits (LE_V = -0.55) and further poses on ranks 16, 22, 41 and 67. The propargyl amide **2g** as well as acrylamide **2f** shows a massive loss of cytotoxic activity compared to the initial hit similar to the unreactive propione amide **2e** and low inhibition in kinase assays.

Table 2. Inhibition of cell viability of MV4-11 cells and FLT3-mutant kinase activity by the indolinone fragment **1g** and the corresponding 5-substituted indolinones **2a** – **i** with chemically reactive electrophilic groups and the analogous unreactive groups.

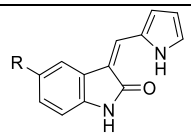 R =	**Compound**	**IC_{50} (MV4-11) / nM**	**Relative Inhibition / %** FLT3(D835Y)		**FLT3(ITD)**
			c = 0.1 µM	**c = 1 µM**	**c = 0.1 µM**
- H	**1g**	380 ± 21	40	86	61
	**2a**	> 1.000	47	90	33
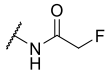	**2b**	845 ± 20	57	92	51
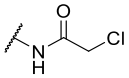	**2c**	72 ± 8	53	87	61
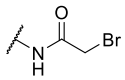	**2d**	653 ± 200	48	92	21
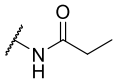	**2e**	> 1.000	15	81	44
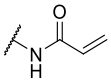	**2f**	> 1.000	29	79	25
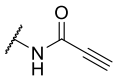	**2g**	709 ± 50	5	58	55
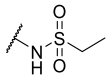	**2h**	> 1.000	13	72	9
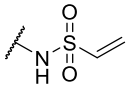	**2i**	67 ± 8	77	96	93

Thus, covalent inhibition is not favorable for acrylamide **2f** though it had been identified in a single pose during virtual screening (rank 1, LE_V = -0.61) obtaining a similar conformation as **2i**. The α-halo acetamides show comparable inhibition of kinase activity in FLT3(D835Y) with the unsubstituted acetamide while a slight preference for the α-chloro acetamide was found inhibiting FLT3(ITD). While the reversible acetamide-substituted indolinone fragment **2a** shows no inhibition of MV4-11 cell viability, the α-fluoro- (**2b**) and α-bromo-substituted (**2d**) acetamides are less active than the initial screening hit **1g**. The α-chloro acetamide **2c** shows similar cytotoxicity as the vinyl sulfonamide **2i**. Having established the structure-activity relationship of indolinone-based irreversible inhibitors we reanalyzed the results from covalent docking to explain disagreements between predicted and confirmed hits.

A possible cause for the false-positive hit acrylamide **2f** might be the negligence of the covalent bond formation as only the reversible fragment and the final covalent complex are modeled during covalent docking. The energy profile of the dihedral angle between the C-C-N plane of the aromatic amine and the C-N-S plane of the reactive group in the top-scored pose of the active vinyl sulfonamide **2i** shows that the energy is close to a local minimum while the dihedral angle is only changed by 3° (56° to 59°) after energy-minimization of the unbound ligand (Figure 2a, S22). The position of the targeted distal carbon atom is slightly shifted by 0.72 Å giving an overall RMSD of 0.49 Å. In contrast, the position of the distal carbon atom in the top-scored docking pose of the inactive acrylamide **2f** is changed by 2.24 Å while the dihedral angle is changed by 39° (overall RMSD 0.89 Å) explaining that the identified hit could not be confirmed experimentally as the modeled conformation of the CRG is unfavorable (Figure 2b). Furthermore, conformational search of unbound ligands **2f** and **2i** shows that the acrylamide warhead is oriented in-plane of the indolinone ring, while the vinyl sulfonamide retains multiple

conformations out-of-plane enabling induced fit to the ATP binding site and vicinity to Cys828 (Figure S23). We further assume that the initial pharmacophore distance of 1.5 Å might be too stringent to allow binding of all warheads, as the α-halo acetamide series was a false negative hit. Consequently, redocking of the α-halo acetamide derivatives **2b** to **2d** was performed using 2 Å ligand pharmacophores. This adjustment led to numerous plausible docking poses and thus showed to be predictive for covalent inhibition by α-halo acetamides (Figure S24).

Characterization of Bisaminopyrimidine-based Irreversible Inhibitors. Similar to the indolinone scaffold, we synthesized 14 inhibitors of the 3- and 4-substituted bisaminopyrimidine scaffold including derivatives with all four types of CRG to include structures predicted as hits and predicted negatives as well as the corresponding reversible substitutions (Table 3). Similarly, the vinyl sulfonamide derivatives **3m** and **3n** of the initial fragment **1f** show massively increased inhibition of MV4-11 cell viability while the corresponding reversible structures **3k** and **3l** show similar cytotoxicity as the reversible fragment **1f**. Inhibition of FLT3 activity shows a comparable increase in inhibition for the reactive derivatives towards FLT3(D835Y) and FLT3(ITD). Interestingly, **3m** shows lower inhibition of FLT3(ITD) but 25-fold increased cytotoxicity in MV4-11 cells suggesting synergistic off-target effects. The 3-methyl derivatives corresponding to **3m** (2 hits, rank 51, 96) and **3n** (3 hits, rank 17, 54, 83) have been identified during virtual screening and redocking of **3m** and **3n** gave similar conformations (Figure S21k – n). These results show that the screening protocol chosen allows predictive hit finding for the bisaminopyrimidine scaffold as well.

Table 3. Inhibition of cell viability of MV4-11 cells and FLT3-mutant kinase activity by the bisaminopyrimidine fragment **1f** and the corresponding 3- and 4-substituted inhibitors **3a** – **n** with chemically reactive electrophilic groups or the analogous unreactive groups.

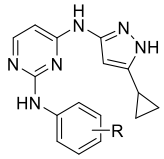 R=	Compound	Substitution	IC_{50} (MV4-11) / nM	Relative Inhibition / % FLT3(D835Y) c = 0.1 µM	FLT3(D835Y) c = 1 µM	FLT3(ITD) c = 0.1 µM
-H	**1f**	-	230 ± 53	52	88	27
	**3a**	3	> 1.000	36	85	54
	3b	4	> 1.000	45	86	82
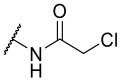	**3c**	3	175 ± 2	33	90	74
	3d	4	141 ± 13	39	93	74
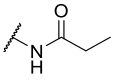	**3e**	3	> 1.000	37	90	66
	3f	4	> 1.000	34	80	22
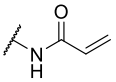	**3g**	3	787 ± 100	22	81	50
	3h	4	521 ± 65	29	84	59
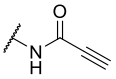	**3i**	3	> 1.000	38	58	2
	3j	4	> 1.000	45	54	17
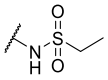	**3k**	3	489 ± 17	32	92	59
	3l	4	129 ± 16	72	96	86
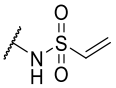	**3m**	3	2.3 ± 0.1	47	90	73
	3n	4	58 ± 16	86	95	99

The acrylamide substitution shows no benefit in cytotoxicity compared to the reversible fragment **1f** while the corresponding reversible inhibitors **3e** and **3f** are almost inactive. During virtual screening the acrylamides have been identified as low-ranked compounds only (**3g**: rank 99 of 102, **3h**: rank 49, 101). The 3- and 4- substituted propargylamides **3i** and **3j** are the least

active inhibitors of this series displaying only neglectable MV4-11 cytotoxicity. Although the propargyl amide **3j** yielded no poses during screening, **3i** was identified (rank 10, 45). Reversible acetamide-substitution of the initial screening hit leads to a loss of cytotoxicity in 3- (**3a**) as well as 4-position (**3b**) while the α-chloro substitutions in **3c** and **3d** leads to a slightly increased cytotoxicity compared to fragment **1f** suggesting a covalent mode of action. However, inhibition of FLT3(D835Y) and FLT3(ITD) was comparable to reversible acetamides **3a** and **3b**, a trend already observed with the indolinone α-chloro-acetamide **2c**, suggesting that kinase screening alone would under-estimate the overall potential of this CRG. In summary, the screening strategy presented gave a hit rate of 73% based on the number of predicted poses (16 correct-positive, 6 false-positive, Figure S25) where all of the vinyl sulfonamide derivatives (3 hits, 10 poses) are validated.

Design of 2nd Generation Indolinone Inhibitors. As the design of covalent binding inhibitors was based on fragmentation of larger lead compounds, we aimed to increase FLT3 inhibition and cytotoxicity by merging the most active irreversible fragments with the parent scaffold. The bisaminopyrimidine scaffold is less suitable for this purpose as the pyrazolyl amine motif may lead to promiscuous kinase inhibitors.[30]

Exemplary, we tested activity of the reversible inhibitors **1f** and **1g** on the far-distant kinases GSK3α and GSK3β yet containing the DFG-1 Cys residue, showing potent inhibition for **1f** (74% and 76% at 1 μM) but only insignificant inhibition by **1g** (12% and -6% at 1 μM). Furthermore, inhibition of cell viability is about 10-fold higher for the meta substituted vinyl sulfonamide **3m** than for the isomer **3n** while inhibition of FLT3 kinase activity shows the opposite trend suggesting that cytotoxicity may arise from synergistic effects by off-target inhibition. Furthermore, **3m** and **3n** are potently cytotoxic towards FLT3wt THP1 cells and

FLT3-negative Jurkat cells (Table 4). Additionally, ligand efficiency in MV4-11 cells is higher for the indolinone derivatives **2c** (-0.34) and **2i** (-0.33) than for the bisaminopyrimidine derivatives **3m** (-0.29) and **3n** (-0.26). Furthermore, the top-scored pose of redocked fragments **2c** and **2i** resemble the orientation of sunitinib in cocrystal structures, where the 3-carbon of pyrrole is exposed to the solvent site of the ATP binding pocket (Figure S26).

Irreversible indolinone scaffolds **2c** and **2i** thus were merged with the parent inhibitor sunitinib by addition of a 2- and 4-methyl group to the pyrrole ring as well as a 3-carboxamide-linked ethylene diethylamine group to give the hybrid structures **4a** and **4b** (Figure 2c). Synthesis was performed similar to procedures described before (SI chapter 2h). Redocking in FLT3 DFG-in was performed using a 2 Å pharmacophore of the indolinone hydrogen bond donor, acceptor and aryl feature. The top-scored binding poses of **4a** and **4b** show comparable binding modes as fragments **2c** and **2i** and sunitinib (Figure 2d, e; S27, S28). The conformation of the solvent-exposed diethylamine group is highly flexible (Figure S29). Receptor-free energy minimization of the ligand shows a distance of the vinyl C^{β} atom of 1.12 Å to its position in the docked pose while the energy plot as a function of the dihedral angle of the sulfonamide is close to its minimum (Figure S30).

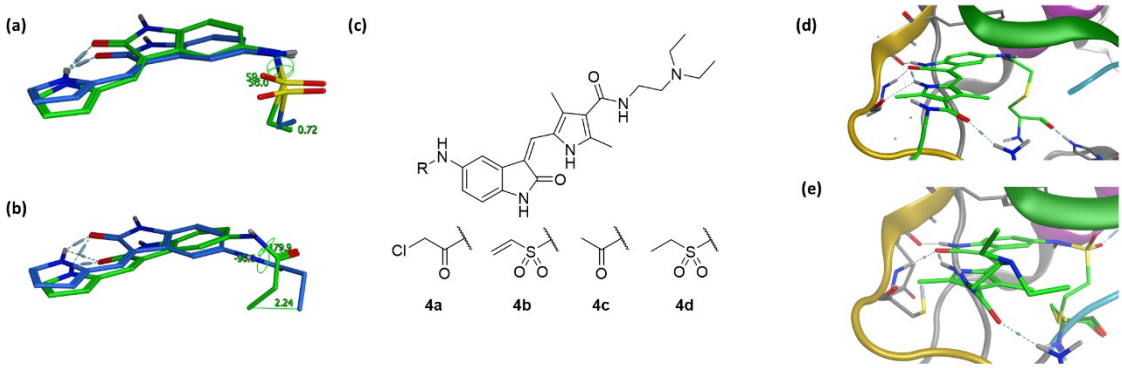

Figure 2. Comparison of the docked (green) and energy-minimized structure (blue) of (a) the active vinyl sulfonamide **2i** and (b) the inactive acrylamide **2f**. (c) Structure of 2nd-generation indolinone inhibitors. (d) Top-scored covalent docking pose of **4a** and (e) **4b**.

Table 4. Inhibition of cell viability in FLT3-mutated (MV4-11), FLT3wt (THP1) and FLT3-negative (Jurkat) cells after 72 h treatment. Inhibition of purified kinase activity is determined at 100 µM ATP and 30 min pre-incubation of kinase and inhibitor using the ADP Glo assay. [a] Half-life towards 100-fold excess of reduced glutathione and 10 µM inhibitor as determined by HPLC. *n.d.* = not determined.

Compound	IC_{50} / nM			Relative Inhibition / %			$t_{1/2\,/\,min}$[a]
	MV4-11 (FLT3(ITD))	THP1 (FLT3wt)	Jurkat (FLT3 neg.)	FLT3(D835Y) c = 0.1 µM	FLT3(D835Y) c = 1 µM	FLT3(ITD) c = 0.1 µM	
4a	21 ± 1	> 1 µM	> 1 µM	71	90	73	218
4b	6.0 ± 0.3	> 1 µM	> 1 µM	95	100	86	51
4c	> 1 µM	*n.d.*	*n.d.*	*n.d.*	*n.d.*	*n.d.*	*n.d.*
4d	643 ± 95	*n.d.*	*n.d.*	32	*n.d.*	*n.d.*	*n.d.*
3m	2.3 ± 0.1	172 ±24	44 ± 5	47	90	73	58
3n	58 ± 16	514 ± 8	298 ± 10	86	95	99	82
Sunitinib	54 ± 1	> 1 µM	> 1 µM	82	96	70	*n.d.*
Hypothemycin	15 ± 3	> 1 µM	> 1 µM	85	92	91	*n.d.*
Crenolanib	12 ± 3	> 1 µM	> 1 µM	95	100	97	*n.d.*

Introduction of the 4-methyl group close to Cys694 changed the position of the sulfonamide group, slightly forcing a strong hydrogen bond donor-acceptor interaction with Lys644. Molecular dynamics simulation of **4b** in complex with the FLT3-DFG-in homology model over 110 ps gives only small RMS deviations (0.5 Å to 1.0 Å) compared to the initial complex concluding that the protein-ligand complex is highly stable (Figure S31). The vinyl sulfonamide substituted sunitinib derivative **4b** shows an increase in cytotoxicity towards MV4-11 cells compared to the irreversible fragment **2i** while the reversible ethyl sulfonamide **4d** is ~100-fold less cytotoxic. Additionally, inhibition of FLT3(D835Y) is further increased, while inhibition

decreases by the ethyl sulfonamide compared to sunitinib. Optimization of the irreversible fragment **2c** to give the sunitinib-derived α-chloro acetamide **4a** yields a 2.5-fold increased cytotoxicity while the unreactive acetamide derivative **4c** is inactive in MV4-11 cells. **4a** and **4b** exhibit both superior cytotoxicity to sunitinib in MV4-11 cells while they retain selectivity towards FLT3wt THP1, NOMO1, U937 as well as FLT3-negative Jurkat cells (Figure S32). In FLT3(ITD)-positive MOLM-14 cells **4b** (IC_{50} = 7.8 nM) is more cytotoxic than **4a** (IC_{50} = 26.4 nM) and **3m** (IC_{50} = 11.6 nM). Vinyl sulfonamide **4b** shows superior cytotoxicity compared to the type I inhibitors midostaurin (~2x), crenolanib (~2x) and hypothemycin (~2.5x) in MV4-11 cells. While increased cytotoxicity in MV4-11 cells by **4b** compared to **4a** correlates with decreased pFLT3 and pSTAT5 levels, **3m** shows higher levels of prosurvival-signaling correlating with decreased inhibition in FLT3 kinase assays (Figures 3a, S33).

Reactivity towards Nucleophiles. Half-life of electrophilic compounds was compared in a HPLC-based assay using 100-fold excess of nucleophiles to investigate the properties of the different CRGs (Figures 3b). While the acrylamide **2f** and α-fluoroacetamide **2b** are highly stable ($t_{1/2}$ > 24 h), the propargylamide **2g** (50 min) as well as the hit-compounds **2c** (384 min) and **2i** (71 min) are less stable. Half-life is decreased by the introduction of the alkaline tertiary amine in **4a** (218 min) and **4b** (52 min). Consequently, pre-incubation of **4b** with a 1000x excess of glutathione (100 nM inhibitor) for 30 min decreased the inhibition of FLT3(D835Y) kinase activity from initial 95% to 68% while incubation for 24h decreases inhibition further (37%). Increase of buffer pH leads to a decrease of half-life (28 min, pH 8) while a decrease of pH increases half-life (130 min, pH 6.8; Figure S34). The α-N-Cbz-protected lysine, serine and threonine amino acids show no conversion with **4b** (pH 7.4).

***Danio Rerio* Embryo Toxicity Assay.** Biocompatibility and toxicologic effects of irreversible FLT3 inhibitors were investigated in *Danio rerio* embryos, that have been shown to be a promising model for drug toxicity screening (Figure 3c).[31] Interestingly, in *Danio rerio* the targeted cysteine (DFG-1) is replaced by an alanine residue, suggesting that off-target rather than FLT3-dependent toxicity can be observed (Table S6, S7). Comparison of the 2-halo-substituted acetamides shows high toxicity for the bromo- **2d** and fluoro- **2b** derivative (10 µM inhibitor), while the chloro- derivative **2c** as well as the reversible acetamide **2a** are not lethal up to 96 h post incubation (120 hpf). The vinyl sulfonamide **2i** as well as hybrid structures **4a** and **4b** are non-toxic at 10 µM comparable to sunitinib, hypothemycin and crenolanib. The bisamino-pyrimidine **3m** shows increased toxicity that is comparable to fragment **1f** suggesting a more promiscuous mode of action.

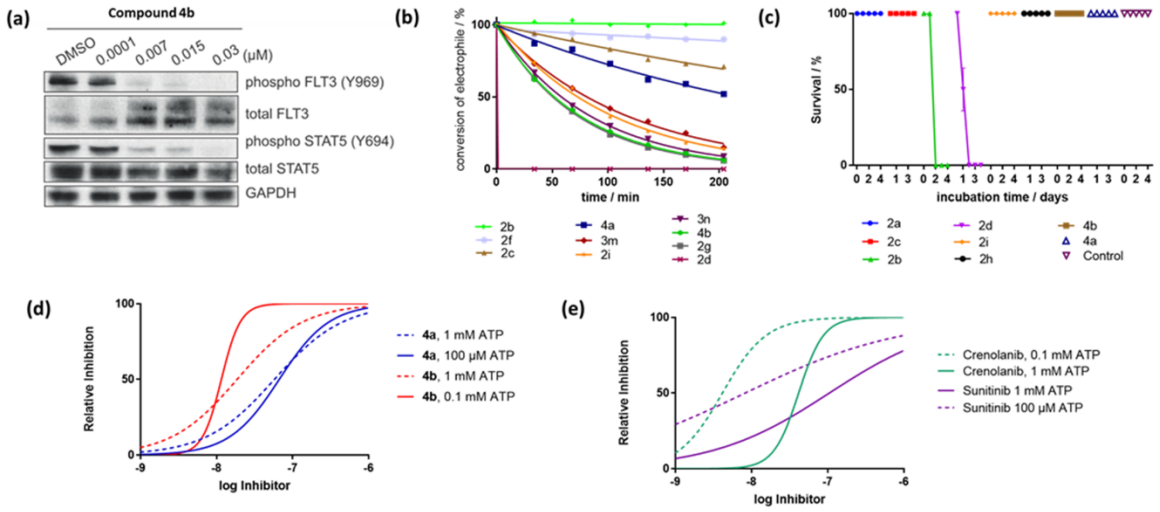

Figure 3. (a) Western Blot analysis of FLT3(Y969) phosphorylation and downstream STAT5 phosphorylation after 1 h incubation with **4b**. (b) Half-life of electrophilic inhibitors towards reduced glutathione (100x excess, pH 7.4). (c) Toxicity of selected inhibitors on Danio rerio embryos (96 hpf, 72 h incubation, 10 µM). (d) Inhibition of FLT3(D835Y) by **4a** and **4b** is

insensitive to high ATP concentrations but is (e) highly dependent on ATP concentration for reversible inhibitors.

ATP- and time-dependent inhibition. We further investigated the ATP- and time-dependency of kinase inhibition by compounds **4a**, **b** and **3m**, **n** in FLT3(D835Y) representing the most active compounds from both series. As expected, the reversible binding FLT3 inhibitors crenolanib and sunitinib show a strong dependency on ATP concentration, where a 10-fold ATP increase (100 µM to 1 mM) leads to an approximately 10-fold decrease of inhibition whereas crenolanib (4.2 nM to 42 nM) remains more potent than sunitinib (8.2 nM to 105 nM, Figure 3d, e). Since irreversible bond formation leads to non-equilibrium-binding only the initial reversible complex, preceding covalent bond formation, is ATP-competitive. Indeed, inhibition of FLT3(D835Y) by **4a** (67 nM at low ATP, 58 nM at high ATP) as well as **4b** (11.6 nM at low ATP to 18.6 nM at high ATP) is less vulnerable to increased ATP concentrations. To our surprise, **3m** and **3n** are highly susceptible to high ATP concentrations suggesting low inactivation kinetics and thus high competitivity to ATP (Figure S35). Additionally, we determined the influence of the pre-incubation time of inhibitor and kinase alone where ATP is not competing with inhibitor binding. As expected, the indolinones **4a** and **4b** as well as the bisaminopyrimidines **3m** and **3n** show increased inhibition of FLT3(D835Y) and FLT3(ITD) when pre-incubation time is increased from 5 min to 30 min (Table S8). To determine the K_i and k_{inact} values of the most potent covalent FLT3 inhibitors **4a** and **4b** we evaluated time-dependent IC_{50} values against FLT3(D835Y) (Figure S36). K_i and k_{inact} have been obtained from the plot $IC_{50}(t)$ vs t by nonlinear regression (see experimental section). We found that **4a** has a lower binding affinity (K_i = 10.14 nM) than **4b** (K_i = 1.98 nM) but a higher inactivation constant (k_{inact}

= 0.0033 / s^{-1} and 0.0017 / s^{-1}). However, determination of K_{inact}/K_i shows that **4b** is a more potent irreversible inhibitor (k_{inact}/K_i = 0.84 μM^{-1} s^{-1}) than **4a** (k_{inact}/K_i = 0.33 μM^{-1} s^{-1})."

Trypsin-digest and MALDI-MS of covalently modified FLT3. Since compounds **4a** and **4b** represent the most active compounds in this study covalent modification of Cys^{828} was confirmed by tryptic in-gel digest of FLT3wt, that was considered to yield the modified octapeptide IC^{828}DFGLAR that could be detected by MALDI mass spectrometry. Standard denaturation and alkylation protocol using dithiothreitol and 2-iodo acetamide allowed detection of the single acetamide-substituted peptide with good agreement of the calculated and found masses and the modeled and measured isotopic pattern (Figure S37 – S41). Subsequent MS/MS allowed detection of numerous fragments of this sequence. Pre-incubation of FLT3wt with **2i**, hypothemycin, **4a** and **4b** allowed detection of calculated masses with small errors confirming covalent modification of Cys828 by the key compounds in this study.

Kinase selectivity of 4b and activity towards resistance-conferring mutations. We chose compound **4b** as lead structure in this project as it shows the strongest inhibition of the isolated kinase and strongest cytotoxicity and further investigated kinase selectivity as well as activity in drug-resistant mutations. Selectivity of the most potent inhibitor **4b** was determined in a panel of 34 kinases at 100 nM inhibitor (Figure 4a). Kinases, that are inhibited by sunitinib, were selected for testing based on available K_d values for sunitinib and for containing the homologous CDFG motif (Table S9, Figure S42). As expected, FLT3 (95%) and FLT3(D835Y) (99%) are potently inhibited. Surprisingly, other kinases of the PDGF receptor family containing the conserved DFG-1 cysteine are significantly less inhibited, including c-KIT (34%), PDGFRα (24%) and

PDGFRβ (14%). This is remarkable as they all share high sequence similarities (>70%) to FLT3 and exhibit single-digit to sub-nanomolar K_d values for sunitinib.[32] Interestingly, less related kinases (30 to 40% sequence similarity) containing the CDFG motif (ERK1, ERK2, GSK3α, GSK3β) are not inhibited at 100 nM **4b** while being reported targets of hypothemycin.[10] **4b** may also covalently modify the homologous serine residue (DFG-1) as the Ret kinase (96%) is strongly inhibited. Interestingly, 5-amino indolinones have been reported to be potent Ret and FLT3 inhibitors while superposition of the FLT3 model and Ret cocrystal structure is in good accordance (RMSD = 0.7 Å, Figure S43).[33] The homolog alanine and glycine residues are tolerated by **4b** (Lyn, Lck, Axl, IRAK1; 93% to 81% inhibition) suggesting that hydrogen bond interactions to the conserved lysine may account for increased affinity compared to sunitinib while a steric clash with $CysS^{\gamma}$ or $SerO^{\gamma}$ is prevented. We further assessed our lead compound **4b** using the KinomeScan screening platform, where numerous FLT3 inhibitors have been assessed before (Figure 4b).[34-35]

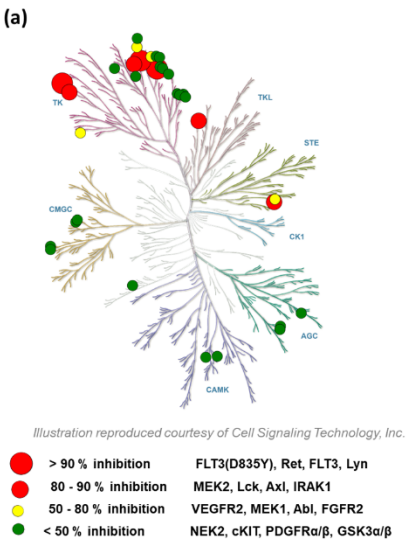

(b)

Inhibitor	FLT3 / K_d / nM				
	D835H	FLT3-ITD	ITD, D835V	ITD, F691L	wt
4b	1,3	5,8	0,83	1,5	2,3
Sunitinib#	4,3	0,99	*n.a.*	*n.a.*	0,41
Midostaurin#	6,8	11	*n.a.*	*n.a.*	11
Sorafenib*	11	95	630	860	13
Quizartinib#	3,7	8,8	*n.a.*	*n.a.*	1,3
VX-680#	14	45	*n.a.*	*n.a.*	6,5
Crenolanib*	0,16	0,26	3,3	22	0,15

*As reported by Zimmerman et al. [34]
As reported by Davis et al. [35]

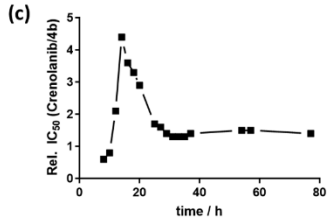

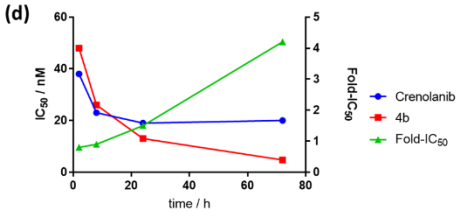

Figure 4. (a) Selectivity of **4b** in a panel of 34 kinases.[36] (b) K_d values of **4b** and inhibitors in clinical trials in a panel of FLT3-mutants. (c) Relative inhibition by time (IC_{50}(crenolanib)/

IC_{50}(**4b**)). (d) Effect of inhibitor wash-out after 2 h, 8 h, 24 h incubation and read-out at 72 h in MV4-11 cells.

Sunitinib and crenolanib show higher affinity towards FLT3wt and FLT3(ITD) than **4b**, while midostaurin is less efficient. Interestingly, sunitinib showed a ~6-fold increased K_d in FLT3(ITD) but inhibition despite cell viability in FLT3-ITD was ~10-fold increased for **4b**. Crenolanib and quizartinib lose affinity towards dual ITD and point-mutated FLT3, while affinity is increased for **4b**. Especially towards the drug-resistant FLT3(ITD, F691L) mutation, **4b** shows a ~15-fold increased affinity compared to crenolanib. Comparison of the affinity of **4b** for the non-autoinhibited (K_d = 2.3 nM) and the autoinhibited state (K_d = 65 nM) of FLT3 shows a 28-fold decrease that is similar to type I inhibitors as sunitinib and midostaurin while type II inhibitors like sorafenib and quizartinib typically give a 100- to 1000-fold shift in affinity.[37]

Time-dependent inhibition of cell viability. To monitor the onset of cytotoxicity we compared crenolanib and **4b** in a real-time cell viability assay with MV4-11 cells (Figure 4c, Figure S44). While cytotoxicity became detectable already after 2 h, robust fitting of cell viability IC_{50} was possible after 8 h for both compounds. Cytotoxicity by **4b** relative to crenolanib was maximal at 18 h (4.4-fold) and plateaus to ~1.5x stronger inhibition for **4b** after 24 h until the end of the assay (77 h). Interestingly, short incubation times (2 h, 8 h) followed by wash-out of the inhibitor and incubation in inhibitor-free medium negatively affects the performance of **4b** compared to crenolanib (Figure 4d). However, potency of **4b** is increased by incubation times longer than 24 h suggesting that rapid *de novo* synthesis of FLT3-ITD may lead to resistance to short incubation times of irreversible inhibitors. However, onset of inhibition by

4b demonstrated by decreased pFLT3 and downstream pSTAT5 levels is in the single-digit nanomolar range after 1 h (Figure 3a).

Evaluation of BODIPY-labeled Activity-based Probes. We further aimed to modify the hit compounds **2c** and **2i** with a boron-dipyrromethene (BODIPY) label attached to the solvent-exposed site of the fragment to image irreversible protein binding similar to a recently reported Ibrutinib-based probe[38] (Figure 5a, b). Synthesis was performed similar to reported work.

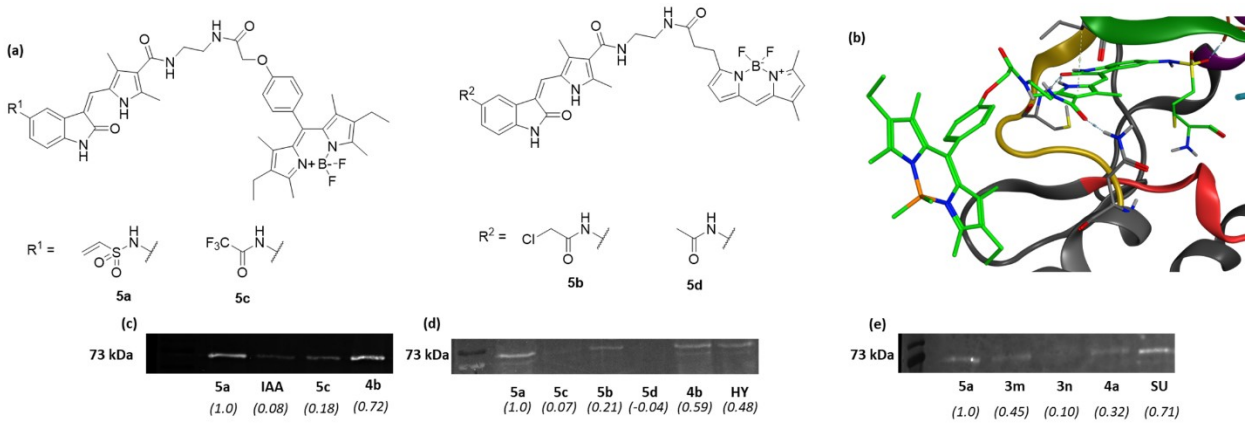

Figure 5. (a) Structure of fluorescent probes **5a** and **5b** and the reversible inhibitors **5c** and **5d**. (b) Binding model of **5a** in FLT3. (c) Western blot of FLT3(D835Y) incubated with **5a** or **5c** (100 µM) and pre-treatment with IAA (10 mM) or **4b** (100 µM) followed by incubation with **5a**. (d) Binding of **5a** – **d** (50 µM) to FLT3(D835Y) and pre-treatment with **4b** and hypothemycin (HY) followed by incubation with **5a**. (e) Binding of **5a** (10 µM) to FLT3(D835Y) and pre-treatment with **3m**, **3n**, **4a** and sunitinib (SU, each 100 µM) followed by incubation with **5a** (10 µM).

Inhibition of FLT3(D835Y) by **5a** (89%) and **5b** (55%) was decreased compared to **4a** and **4b** (1 μM inhibitor) but still superior to the corresponding reversible inhibitors **5c** (34%) and **5d** (23%) (Figure S45). Incubation of FLT3(D835Y) with probes **5a** - **d** and subsequent standard gel electrophoresis and Western blot allows fluorescent detection of covalent binding for **5a** and **5b** (50 μM, Figure 5c, d, Figure S46) while acetamide **5d** shows no fluorescence. Interestingly, trifluoroacetamide **5c** shows similar binding compared to **5b** (18% at 100 μM and 7% at 50 μM; relative integrated density compared to **5a**). We thus pre-treated FLT3(D835Y) with reversibly and irreversibly acting inhibitors following incubation with fluorescent probe **5a** that gave the highest fluorescence signal and signal to background ratio. Treatment of FLT3(D835Y) with 10 mM IAA almost completely abrogated fluorescence after treatment with **5a** (100 μM). Incubation with **4b** (100 μM) gave a small decrease of fluorescence with 100 μM of probe **5a** (-28%) while incubation with 50 μM probe decreased fluorescence signal further (-41%) and comparable to treatment with hypothemycin (-52%). A similarly decreased fluorescence was observed after pre-incubation with bisaminopyrimidines **3m** (-55%), **3n** (-90%) and indolinone **4a** (-68%). Incubation with the reversible inhibitor sunitinib (-29%) slightly decreases fluorescence suggesting covalent binding of the probe in the ATP site where the 10x excess of pre-treated inhibitor strongly competes with the reversible complex preceding covalent binding of the irreversible probe (Figure 5e). Additionally, gastrointestinal uptake of probes **5a** and **5b** could be detected in *Danio rerio* embryos (Figure S47).

Conclusions and Perspective

In summary, we have discovered irreversible binding FLT3 inhibitors that overcome drug-resistant mutations of FLT3. A focused screening library was designed by attachment of chemically reactive groups to potent reversible binding fragments. Subsequent covalent docking

identified two privileged scaffolds that gave numerous FLT3 inhibitors with improved cytotoxicity in FLT3-driven cell lines. Hybridization with the parental sunitinib scaffold gave the most potent compound **4b** (BSc5371) that shows increased cytotoxicity in comparison to drugs in current clinical trials and is selective over closely related kinases. Subsequent development of an activity-based probe enabled imaging of covalent binding and competition with non-fluorescent inhibitors. The screening strategy presented here is adaptable to many drug targets and may serve as a blueprint for the rational in silico design of covalent drugs enabling more time- and cost-efficient drug discovery.

Experimental Section

Covalent Virtual Screening and Filter Strategy

Homology Model

The protein sequence of FLT3 (PDB: 1RJB) and the structure of cKIT in complex with ADP (PDB: 1PKG) was obtained from the protein databank. Amino acid residues that are only described in one of the models and are distant from the ATP-binding pocket were discarded (see Table S1 and Figure S1). The homology model was built using Molecular Operating Environment 2014.09 (MOE, Chemical Computing Group). Protein sequences were aligned and the sequence of 1RJB was modeled on the template 1PKG using 25 mainchain models and the Amber12:EHT forcefield. RMSD between the template and the final model is 0.01 Å. The Ramachandran Plot of the final model displays four geometric outliers that are all distant from the ATP-binding pocket and were not further optimized.

Reversible Docking

Initial pharmacophores for the 13 selected reversible inhibitor scaffolds were built using a superposition of reported crystal structures and the FLT3 DFG-*in* homology model to enable robust evaluation of the most likely reversible binding pose (Figures S6 to S18). Input structures were drawn using ChemBioDraw Ultra 14.0 and energy minimized using MOE and the MMFF94x forcefield. The final selected docking pose that serves as a template was used to define the pharmacophore for the covalent virtual screening.

Covalent Docking using Docktite

All compounds studied were docked in the ATP-binding site where the reversible inhibitor serves as a site indicator and defines the pharmacophore. Covalent docking was performed using the Docktite SVL script set for MOE. Input structures were generated by modification of the reversible docked inhibitor scaffold with a chemical reactive group at an appropriate site to give 128 inhibitors (see figure S5). The chemical reactive groups are tagged and attached to the covalent attachment point to give 160 sidechain-attached ligands that served as ligands for covalent docking. Pharmacophores were generated automatically regarding the features of the covalent attachment point (R = 0.4 Å) and have been enhanced using aryl and hydrogen-bond donor and acceptor features (R = 1.5 Å, see figure S6B to S18B). The pharmacophore feature of the nucleophilic sulfur atom is increased to 3.0 Å to allow conformational flexibility of the attachment point, while the other heavy atoms of Cys828 are unchanged to resemble the initial input conformation of the homology model. The Cys828 residue and the N- and C-terminal amide group were removed from the receptor for covalent docking. Docking was performed using MOE´s rigid receptor docking function and the Amber12:EHT forcefield. 5000 conformations of the attached ligands are sampled and filtered by the pharmacophore model.

Rescoring of the placements was performed using the London dG scoring function and 100 poses are subjected to grid-based minimization and rescored using London dG. The force constant of the pharmacophore restraint was set to 1e+9. The docking was performed in batch jobs and was finished after approximately 48 h using a custom-built 64-bit computer system (Intel i7-4790K CPU 4*4GHz, 8 GB Ram 2800 MHz). The attached sidechain was then cleaved from the inhibitor using Docktite to allow more robust rescoring of the ligand. 831 poses have been retained and are subjected to the filter strategy.

Filter strategy

In the first step for scaffold selection, DSX rescoring was performed using the linux-based standalone version. Ligands that contain any of the three characteristic backbone interactions with the hinge region (gatekeeper +1 residue Glu692 backbone donor interaction; and/or gatekeeper +3 residue Cys694 backbone donor/acceptor interaction) are selected using the Protein-Ligand Interaction Fingerprints (PLIFs) function of MOE (*404 poses remaining*). From these poses only the top 5 poses of each ligand are retained (*319 poses remaining*). In the last filter step, ligands with a ligand efficiency of more than -0.5 HA/kcal are discarded (LE_V = (London dG Score) / (number of heavy atoms). Redocking of the experimental validated hits was done like the screening method using forcefield minimization and an enhanced pharmacophore radius of the scaffold pharmacophore (R = 2Å).

Molecular Dynamics

The molecular dynamics simulations of **4b** were performed using MOE2016.09 and the NPA algorithm[39] starting from the top-scored docking pose of **4b** in the FLT3 DFG-in homology model. 10 picoseconds of equilibration are followed by a 100 ps production step using a time step of 0.1 ps. All bond lengths have been constrained. Time step for the equation of motions

was set to 0.001. Temperature was set to 300K. The time-dependent RMSD values are given in the SI (Figure S31).

Chemistry

General remarks

Solvents and chemicals were purchased from ABCR, Acros Organics, Alfa Aesar, Deutero Gmbh, Fluka, Grüssing Gmbh, Merck, Carl Roth, Sigma-Aldrich and VWR and were used without further purification unless stated otherwise. Qualitative analytical thin layer chromatography was performed using silica gel 60 plates with fluorescent indicator F254 from Merck. Developed plates were dried and observed under UV light (254 or 365 nm). Silica chromatography was performed using silica gel 60 (0.015 – 0.04 mm particle size) from Merck and an isocratic solvent mixture. Flash chromatography was performed using a Teledyne ISCO Combiflash Rf 4x system with pre-packed silica columns obtained from Telos. The column was conditioned with solvent to the starting concentration of the gradient. Peaks were detected at 214/254 nm (reversed-phase chromatography) or 254/280 nm (normal phase chromatography). ^{1}H and ^{13}C-NMR spectra were recorded on a Bruker AR 300 (^{1}H at 300 MHz, ^{13}C at 75 MHz) or a Bruker DRX 500 spectrometer (^{1}H at 500 MHz, ^{13}C at 126 MHz). The specific frequency and solvents are stated for each experiment. Chemical shifts δ are expressed in ppm using the solvent residual proton signal as reference. Signal splitting patterns are described as singlet (s), doublet (d), triplet (t), quartet (q), multiplet (m) or a combination thereof. Coupling constants *J* are rounded to one decimal place and given in Hz. The spectra were evaluated using MestReNova 11 by Mestrelab Research. High Performance Liquid Chromatography was performed with an Agilent 1100 system using a phenomenex synergi polar reversed phase column (4 µm particle size, 150 x 3.0 mm, pore size 80 Å) connected to a variable wavelength detector. Mobile phase

consists of water/acetonitrile + 0.1% trifluoro acetic acid forming a linear gradient starting with 30% water (held for 1 minute) increased to 90% acetonitrile over 10 min and held for one min with a constant flow of 1 ml/min. Microwave assisted synthesis were performed in a Biotage Initiator plus microwave reactor using the conditions stated in the corresponding experiments. EI-MS spectra were recorded on a double focused mass spectrometer MAT95. ESI-MS was obtained using a Bruker Daltonics qTOF spectrometer. All compounds used in biochemical assays have a purity of more than 95% as determined by HPLC and are reported at the corresponding experiments.

***N*^{4}-(5-methyl-1H-pyrazol-3-yl)-*N*^{2}-phenylpyrimidine-2,4-diamine (1a).** To a solution of 2-chloro-*N*-(5-methyl-1*H*-pyrazol-3-yl)pyrimidin-4-amine (150 mg, 0.72 mmol, 1.0 equiv) in *n*-butanol (4 ml) was added aniline (67 mg, 0.72 mmol, 1.0 equiv) and 37% hydrochloric acid (20 µl). The mixture was stirred for 24 h at 100°C, cooled to room temperature and kept at 4°C overnight. The precipitate was isolated by filtration, washed with cyclohexane and dichloromethane and purified by reversed-phase flash chromatography (acetonitrile/H_2O = 10 to 100%) to give **1a** as a colorless amorphous solid. Yield: 115 mg, 0.432 mmol, 60%. ^{1}H NMR (500 MHz, DMSO-d_6) δ_H (ppm) = 12.40 (s, 1H), 11.03 (s, 1H), 10.65 (s, 1H), 8.00 (d, J = 7.1 Hz, 1H), 7.59 (d, J = 7.7 Hz, 2H), 7.44 (t, J = 7.9 Hz, 2H), 7.24 (t, J = 7.4 Hz, 1H), 6.54 (s, 1H), 6.22 (s, 1H), 2.20 (s, 3H). ^{13}C NMR (126 MHz, DMSO-d_6) δ_C (ppm) = 159.9, 159.4, 159.1, 153.1, 146.0, 139.1, 137.0, 128.9, 124.8, 117.9, 96.8, 10.6. MS (EI): m/z = 266 $[M]^+$. HPLC (254 nm): t_R = 1.827 min (99.4713%).

(*Z*)-3-Benzylideneindolin-2-one (1b).[40] To a solution of indolin-2-one (200 mg, 1.5 mmol, 1.0 equiv) and benzaldehyde (159 mg, 1.502 mmol, 1.0 equiv) in tetrahydrofuran (4 ml), piperidine (25 µl) was added and the mixture was heated in a microwave reactor at 120°C

for 90 min. The solvent was evaporated, and the crude product purified by flash chromatography (dichloromethane/MeOH = 0 to 10%) to yield the product as a yellow amorphous solid. Yield: 122 mg, 0.55 mmol, 37%. ^{1}H NMR (500 MHz, DMSO-d_6) δ_H (ppm) = 10.61 (s, 1H), 7.75 – 7.70 (m, 2H), 7.66 (s, 1H), 7.60 – 7.45 (m, 4H), 7.25 (td, J = 7.7, 1.2 Hz, 1H), 6.95 – 6.78 (m, 2H). ^{13}C NMR (126 MHz, DMSO-d_6) δ_C (ppm) = 168.6, 143.0, 135.7, 134.5, 130.2, 129.6, 129.2, 128.7, 127.7, 122.3, 121.1, 120.9, 110.1. MS (ESI): m/z = 244.08 $[M+Na]^+$. HPLC (254 nm): t_R = 6.412 min (96.7002%).

3-Phenylimidazo[1,2-a]pyridine (1c).[41] To a solution of imidazo[1,2-a]pyridine (100 mg, 0.846 mmol, 1.0 equiv) and bromobenzene (251 mg, 1.69 mmol, 2.0 equiv) in dry DMF (4 ml) was added $Pd(OAc)_2$ (19 mg, 0.085 mmol, 0.1 equiv) and KOAc (166 mg, 1.69 mmol, 2.0 equiv) and the mixture was degassed under argon for 30 min. The reaction mixture was stirred in a microwave reactor at 160°C for 1 h. Then it was cooled to room temperature poured, in a mixture of saturated aqueous $NaHCO_3$ solution (10 mL) and ethyl acetate (20 ml). The organic layer was washed with saturated aqueous sodium bicarbonate solution (2 x 10 ml) and water (3 x 10 ml), dried over $MgSO_4$ and concentrated under reduced pressure. The crude product was purified by reversed-phase flash chromatography (acetonitrile/H_2O = 10 to 100%) to give **1c** as a colorless amorphous solid. Yield: 95 mg, 0.49 mmol, 58%. ^{1}H NMR (500 MHz, $CDCl_3$ + 10% DMSO-d_6) δ_H (ppm) = 8.41 (d, J = 6.8 Hz, 1H), 8.15 (d, J = 9.0 Hz, 1H), 7.84 (s, 1H), 7.77 (t, J = 7.9 Hz, 1H), 7.59 – 7.46 (m, 5H), 7.29 (t, J = 6.9 Hz, 1H). ^{13}C NMR (126 MHz, $CDCl_3$ + 10% DMSO-d_6) δ_C (ppm) = 140.3, 132.5, 130.8, 129.9, 129.1, 127.3, 124.9, 124.6, 121.0, 117.3, 114.2. MS (EI): m/z = 194 $[M]^+$. HPLC (254 nm): t_R = 5.602 min (95.8210%).

6,7-Dimethoxy-*N*-phenylquinazolin-4-amine (1d). To a solution of 4-chloro-6,7-dimethoxyquinazoline (50 mg, 0.22 mmol, 1.0 equiv) in isopropyl alcohol (2 ml) was added aniline (32 mg, 0.34 mmol, 1.55 equiv). The mixture was refluxed for 16 h and cooled to room temperature. The precipitate formed was isolated by filtration and washed with ethyl acetate (1 ml) twice to give the product as a colorless amorphous solid. Yield: 62 mg, 0.216 mmol, 98%. ^{1}H NMR (500 MHz, DMSO-d_6) δ_H (ppm) = 11.51 (s, 1H), 8.81 (s, 1H), 8.40 (s, 1H), 7.79 – 7.66 (m, 2H), 7.50 (t, J = 7.9 Hz, 2H), 7.41 (s, 1H), 7.38 – 7.29 (m, 1H), 4.04 (s, 3H), 4.00 (s, 3H). ^{13}C NMR (126 MHz, DMSO-d_6) δ_C (ppm) = 158.2, 156.2, 150.2, 148.6, 136.86, 135.4, 129.5, 128.7, 126.3, 124.9, 107.2, 104.1, 99.7, 57.0, 56.4. MS (EI): m/z = 281 $[M]^+$. HPLC (254 nm): t_R = 5.997 min (97.2261%).

3,5-Diphenyl-1H-pyrrolo[2,3-b]pyridine (1e). 3,5-Diphenyl-1-tosyl-1*H*-pyrrolo[2,3-b]-pyridine (56 mg, 0.13 mmol, 1.0 equiv) was dissolved in a mixture of MeOH (15 ml) and aqueous 4 N sodium hydroxide (0.2 ml) and stirred at 50°C for 24 h. The reaction mixture was cooled to room temperature and adjusted to pH 5-6 by addition of aqueous 2 N hydrochloric acid. The mixture was concentrated and treated with water (10 ml) and ethyl acetate (10 ml). The aqueous layer was extracted with ethyl acetate (10 ml) three times and the combined organic layers were washed with brine, dried over $MgSO_4$ and the solvent was evaporated. The crude product was purified by silica chromatography (cyclohexane/ethyl acetate = 1/1) to give the title compound as a colorless amorphous solid. Yield: 26 mg, 0.095 mmol, 73%. ^{1}H NMR (500 MHz, DMSO-d_6) δ_H (ppm) = 11.99 (s, 1H), 8.57 (d, J = 2.1 Hz, 1H), 8.43 (d, J = 2.0 Hz, 1H), 7.91 (d, J = 2.6 Hz, 1H), 7.78 (ddd, J = 12.7, 8.2, 1.1 Hz, 4H), 7.47 (ddd, J = 19.7, 10.9, 4.6 Hz, 4H), 7.41 – 7.35 (m, 1H), 7.30 – 7.23 (m, 1H). ^{13}C NMR (126 MHz, DMSO-d_6) δ_C (ppm) = 148.6, 141.9,

139.0, 134.9, 128.9, 128.9, 128.8, 127.1, 126.9, 126.39, 125.7, 125.4, 124.6, 117.3, 114.7. MS (EI): m/z = 270 $[M]^+$. HPLC (254 nm): t_R = 2,653 min (97,4023%).

***N*⁴-(5-Cyclopropyl-1*H*-pyrazol-3-yl)-*N*²-phenylpyrimidine-2,4-diamine (1f).** To a solution of 2-chloro-*N*-(5-cyclopropyl-1H-pyrazol-3-yl)pyrimidin-4-amine (200 mg, 0.849 mmol, 1.0 equiv) in *n*-butanol (3.2 ml) was added aniline (79 mg, 0.849 mmol, 1.0 equiv) and 37 % hydrochloric acid (40 µl). The mixture was stirred for 24 h at 100°C and subsequently cooled to room temperature and kept at 4°C overnight. The precipitate was isolated by filtration, washed with cyclohexane and dichloromethane and purified by reversed-phase flash chromatography (acetonitrile/H_2O = 10 to 100%) to give **1f** as a colorless amorphous solid. Yield: 159 mg, 0.54 mmol, 64%. ^{1}H NMR (500 MHz, DMSO-d_6) δ_H (ppm) = 12.48 (s, 1H), 11.20 (s, 1H), 10.68 (s, 1H), 8.21 – 7.81 (m, 1H), 7.56 – 7.47 (m, 2H), 7.44 (t, *J* = 7.7 Hz, 2H), 7.27 (d, *J* = 7.4 Hz, 1H), 6.46 (s, 1H), 6.04 (s, 1H), 1.83 (dt, *J* = 8.8, 3.8 Hz, 1H), 1.11 – 0.89 (m, 2H), 0.55 (s, 2H). ^{13}C NMR (126 MHz, DMSO-d_6) δ_C (ppm) = 176.6, 159.7, 157.4, 152.7, 146.5, 145.7, 142.2, 136.5, 129.0, 125.4, 123.4, 99.2, 93.3, 7.9, 6.7. MS (ESI): m/z = 293.1 $[M+H]^+$. HPLC (254 nm): t_R = 1.778 min (98.6020%).

(*Z*)-3-((1*H*-Pyrrol-2-yl)methylene)indolin-2-one (1g).[40] To a solution of **i**ndolin-2-one (200 mg, 1.5 mmol, 1.0 equiv) and 1*H*-pyrrole-2-carbaldehyde (142 mg, 1.502 mmol, 1.0 equiv) in tetrahydrofuran (4 ml), piperidine (25 µl) was added and the mixture was heated in a microwave reactor at 120°C for 90 min. The solvent was evaporated, and the crude product purified by flash chromatography (dichloromethane/MeOH = 0 to 10%) to yield the product as a yellow amorphous solid. Yield: 131 mg, 0.62 mmol, 42%. ^{1}H NMR (300 MHz, DMSO-d_6) δ_H (ppm) = 13.34 (s, 1H), 10.88 (s, 1H), 7.74 (s, 1H), 7.66 – 7.60 (m, 1H), 7.35 (td, *J* = 2.7, 1.4 Hz, 1H), 7.15 (td, *J* = 7.6, 1.2 Hz, 1H), 7.00 (td, *J* = 7.6, 1.1 Hz, 1H), 6.89 (dt, *J* = 7.6, 0.9 Hz, 1H),

6.84 (dt, *J* = 3.6, 1.7 Hz, 1H), 6.36 (dt, *J* = 3.7, 2.3 Hz, 1H). ^{13}C NMR (75 MHz, DMSO-d_6) δ_C (ppm) = 169.2, 138.9, 129.5, 126.8, 126.3, 125.6, 125.1, 121.2, 120.2, 118.5, 116.8, 111.4, 109.5. MS (EI): m/z = 210.0 $[M]^+$. HPLC (254 nm): t_R = 2.967 min (98.4849%).

(*Z*)-*N*-(3-((1*H*-pyrrol-2-yl)methylene)-2-oxoindolin-5-yl)acetamide (2a). To a solution of (*Z*)-3-((1*H*-pyrrol-2-yl)methylene)-5-aminoindolin-2-one (100 mg, 0.444 mmol, 1.0 equiv) in THF (20 ml) at 0°C was added triethylamine (123 µl, 0.888 mmol, 2.0 equiv) and acetyl chloride (35 µl, 0.488 mmol, 1.1 equiv). The solution was warmed to room temperature and stirred for 2 h. The reaction was quenched by the addition of brine (20 ml) and ethyl acetate (20 ml) and the organic layer was washed with 0.1 N aqueous HCl (2 x 10 ml) and 0.1 N aqueous NaOH solution (2 x 10 ml). The organic layer was dried over Na_2SO_4, the solvent was removed, and the crude product was purified by flash chromatography (dichloromethane/MeOH = 1 to 10%) to give the product as a yellow amorphous solid. Yield: 69 mg, 0.257 mmol, 58%. ^{1}H NMR (500 MHz, DMSO-d_6) δ_H (ppm) = 13.36 (s, 1H), 10.80 (s, 1H), 9.80 (s, 1H), 7.92 (d, *J* = 2.0 Hz, 1H), 7.60 (s, 1H), 7.37 (dt, *J* = 4.1, 2.0 Hz, 1H), 7.20 (d, *J* = 8.3, 2.0 Hz, 1H), 6.93 (dt, *J* = 3.5, 1.7 Hz, 1H), 6.83 (d, *J* = 8.3 Hz, 1H), 6.37 (dt, *J* = 3.6, 2.4 Hz, 1H), 2.05 (s, 3H). ^{13}C NMR (126 MHz, DMSO-d_6) δ_C (ppm) = 169.3, 167.8, 134.9, 133.5, 129.5, 126.1, 125.7, 125.1, 120.6, 118.8, 117.0, 111.4, 110.5, 109.4, 40.1, 39.9, 39.7, 39.5, 39.4, 39.2, 39.1, 23.8. MS (ESI) m/z = 268.1 $[M+H]^+$. HPLC (254 nm): t_R = 3.843 min (100.0000%).

(*Z*)-*N*-(3-((1*H*-pyrrol-2-yl)methylene)-2-oxoindolin-5-yl)-2-fluoroacetamide (2b). 2d (124 mg, 0.355 mmol, 1.0 equiv) and potassium fluoride (206 mg, 3.55 mmol, 10.0 equiv) were suspended in diethylene glycol (5 ml) and stirred at 130°C for 5 h. The reaction mixture was cooled to room temperature and diluted with water (100 ml), extracted with dichloromethane (2 x 50 ml), dried over Na_2SO_4 and the solvent was evaporated. The residue was purified by

silica chromatography (dichloromethane/MeOH=20/1) to give the title compound as a yellow amorphous solid. Yield: 35 mg, 0.123 mmol, 35%. ^{1}H NMR (300 MHz, DMSO-d_6) δ_H (ppm) = 13.34 (s, 1H), 10.86 (s, 1H), 9.97 (s, 1H), 7.93 (d, J = 2.0 Hz, 1H), 7.62 (s, 1H), 7.49 – 7.24 (m, 2H), 7.01 – 6.78 (m, 2H), 6.36 (dt, J = 3.8, 2.3 Hz, 1H), 5.06 (s, 1H), 4.90 (s, 1H). ^{13}C NMR (75 MHz, DMSO-d_6) δ_C (ppm) = 169.3, 165.6, 165.4, 135.5, 131.9, 129.4, 126.3, 125.8, 125.1, 120.8, 119.7, 116.7, 111.4, 109.4, 81.2, 78.8. MS (ESI) m/z = 286.1 $[M+H]^+$. HPLC (254 nm): t_R = 4.282 min (95.1175%).

(*Z*)-*N*-(3-((1*H*-pyrrol-2-yl)methylene)-2-oxoindolin-5-yl)-2-chloroacetamide (2c). To a solution of (*Z*)-3-((1*H*-pyrrol-2-yl)methylene)-5-aminoindolin-2-one (106 mg, 0.47 mmol, 1.0 equiv) in THF (15 ml) at 0°C was added pyridine (57 µl, 0.71 mmol, 1.5 equiv) and chloro acetyl chloride (49 µl, 0.611 mmol, 1.3 equiv). The solution was warmed to room temperature and stirred for 1 h. The reaction was quenched by the addition of brine (20 ml) and ethyl acetate (20 ml) and the organic layer was washed with saturated aqueous sodium bicarbonate solution (20 ml) and brine (20 ml), dried with Na_2SO_4 and the solvent was evaporated. The residue was purified by silica chromatography (dichloromethane/MeOH=20/1) to give the title compound as a yellow amorphous solid. Yield: 53 mg, 0.18 mmol, 37%. ^{1}H NMR (500 MHz, DMSO-d_6) δ_H (ppm) = 13.42 (s, 1H), 10.66 (s, 1H), 10.07 (s, 1H), 7.89 (d, J = 1.9 Hz, 1H), 7.47 (s, 1H), 7.23 – 7.17 (m, 2H), 6.83 – 6.76 (m, 2H), 6.31 (dt, J = 3.6, 2.3 Hz, 1H), 4.17 (s, 2H). ^{13}C NMR (126 MHz, DMSO-d_6) δ_C (ppm) = 169.3, 164.2, 135.5, 132.3, 129.5, 125.9, 125.2, 124.9, 120.1, 118.8, 117.0, 111.2, 110.5, 109.3, 43.3. MS (ESI) m/z = 302.1 $[M+H]^+$. HPLC (254 nm): t_R = 4.985 min (96.1842%).

(*Z*)-*N*-(3-((1*H*-pyrrol-2-yl)methylene)-2-oxoindolin-5-yl)-2-bromoacetamide (2d). To a solution of (*Z*)-3-((1*H*-pyrrol-2-yl)methylene)-5-aminoindolin-2-one (247 mg, 1.1 mmol, 1.0 equiv)

in dry THF (20 ml) at 0°C was added diisopropylethylamine (382 µl, 2.2 mmol, 2.0 equiv) and bromo acetyl bromide (242 mg, 1.2 mmol, 1.1 equiv). The solution was warmed to room temperature and stirred for 1 h. The reaction was quenched by the addition of brine (20 ml) and ethyl acetate (40 ml), the organic layer was washed with saturated aqueous sodium bicarbonate solution (20 ml) and brine (20 ml), dried with Na_2SO_4 and the solvent was evaporated. The residue was purified by silica chromatography (dichloromethane/MeOH=20/1) to give the title compound as a yellow amorphous solid. Yield: 163 mg, 0.472 mmol, 47%. ^{1}H NMR (300 MHz, DMSO-d_6) δ_H (ppm) = 13.34 (s, 1H), 10.86 (s, 1H), 10.27 (s, 1H), 7.93 (d, J = 2.0 Hz, 1H), 7.65 (s, 1H), 7.36 (q, J = 2.1 Hz, 1H), 7.20 (dd, J = 8.4, 2.0 Hz, 1H), 7.00 – 6.77 (m, 2H), 6.36 (dt, J = 4.1, 2.3 Hz, 1H), 4.04 (s, 2H). ^{13}C NMR (75 MHz, DMSO-d_6) δ_C (ppm) = 169.2, 164.4, 135.4, 132.6, 129.5, 126.4, 125.9, 125.2, 120.8, 118.9, 116.7, 111.5, 110.5, 109.6, 30.4. MS (ESI) m/z = 346.03 $[M+H]^+$. HPLC (254 nm): t_R = 5.145 min (95.9804%).

(*Z*)-*N*-(3-((1*H*-pyrrol-2-yl)methylene)-2-oxoindolin-5-yl)propionamide (2e). To a solution of (*Z*)-3-((1*H*-pyrrol-2-yl)methylene)-5-aminoindolin-2-one (57 mg, 0.253 mmol, 1.0 equiv) in acetonitrile (4 ml) was added triethylamine (35 µl, 0.235 mmol, 1.0 equiv), 1-(3-dimethylaminopropyl)-3-ethylcarbodiimide hydrochloride (97 mg, 0.51 mmol, 2.0 equiv) and propanoic acid (23 µl, 0.304 mmol, 1.2 eq). The reaction was stirred at room temperature overnight and water (20 ml) and ethyl acetate (20 ml) were added. The organic layer was washed with saturated aqueous sodium bicarbonate solution (20 ml) and brine (20 ml), dried over sodium sulfate and the solvent was evaporated. The residue was purified by silica chromatography (dichloromethane/MeOH=20/1) to give the title compound as a yellow amorphous solid. Yield: 21 mg, 0.075 mmol, 30%. ^{1}H NMR (500 MHz, DMSO-d_6) δ_H (ppm) = 13.55 – 13.29 (m, 1H), 10.52 (s, 1H), 9.50 (s, 1H), 7.96 – 7.91 (m, 1H), 7.39 (s, 1H), 7.18 – 7.13 (m, 2H), 6.76 (d, J =

8.3 Hz, 1H), 6.72 (dt, *J* = 3.6, 1.7 Hz, 1H), 6.30 (dt, *J* = 3.7, 2.3 Hz, 1H), 2.33 (q, *J* = 7.6 Hz, 2H), 1.15 (t, *J* = 7.6 Hz, 3H). ^{13}C NMR (126 MHz, DMSO-d_6) δ_C (ppm) = 171.8, 169.4, 134.9, 133.2, 129.5, 125.5, 125.0, 124.6, 119.7, 118.6, 117.3, 111.1, 110.4, 109.2, 29.5, 9.6. MS (EI) m/z = 281 $[M]^+$. HPLC (254 nm): t_R = 4.881 min (95.0225%).

(*Z*)-*N*-(3-((1*H*-pyrrol-2-yl)methylene)-2-oxoindolin-5-yl)acrylamide (2f). To a solution of (*Z*)-3-((1*H*-pyrrol-2-yl)methylene)-5-aminoindolin-2-one (153 mg, 0.679 mmol, 1.0 equiv) in dichloromethane (25 ml) at 0°C was added triethylamine (188 µl, 1.358 mmol, 2.0 equiv) and acryloyl chloride (60 µl, 0.75 mmol, 1.1 equiv). The solution was warmed to room temperature and stirred overnight. The reaction was quenched by the addition of water (20 ml) and ethyl acetate (20 ml) and the organic layer was washed with saturated aqueous sodium bicarbonate solution (2 x 20 ml) and brine (20 ml) and dried over Na_2SO_4. The solvent was evaporated, and the crude product was purified by silica chromatography (dichloromethane/MeOH = 20/1) to give the title compound as a yellow amorphous solid. Yield: 65 mg, 0.232 mmol, 34%. ^{1}H NMR (500 MHz, DMSO-d_6) δ_H (ppm) = 13.33 (s, 1H), 10.83 (s, 1H), 10.10 (s, 1H), 8.00 (d, *J* = 1.9 Hz, 1H), 7.63 (s, 1H), 7.45 – 7.24 (m, 2H), 7.02 – 6.80 (m, 2H), 6.45 (dd, *J* = 16.9, 10.1 Hz, 1H), 6.37 – 6.15 (m, 1H), 5.75 (dd, *J* = 10.1, 2.0 Hz, 1H). ^{13}C NMR (126 MHz, DMSO-d_6) δ_C (ppm) = 169.3, 163.0, 135.2, 133.0, 131.9, 129.4, 126.4, 126.3, 125.9, 125.2, 120.8, 119.0, 116.7, 111.5, 110.6, 109.6. MS (ESI) m/z = 280.5 $[M+H]^+$. HPLC (254 nm): t_R = 4.752 min (95.2080%).

(*Z*)-*N*-(3-((1*H*-pyrrol-2-yl)methylene)-2-oxoindolin-5-yl)propionamide (2g). To a solution of (*Z*)-3-((1*H*-pyrrol-2-yl)methylene)-5-aminoindolin-2-one (115 mg, 0.51 mmol, 1.0 equiv) in acetonitrile (4 ml) at 0°C was added triethylamine (71 µl, 0.51 mmol, 1.0 equiv), 1-(3-dimethylaminopropyl)-3-ethylcarbodiimide hydrochloride (195 mg, 1.02 mmol, 2.0 equiv) and

propargylic acid (38 µl, 0.612 mmol, 1.2 equiv) and stirred overnight at room temperature. The reaction was quenched by the addition of brine (20 ml) and ethyl acetate (20 ml) and the organic phase was washed with 0.1 N aqueous HCl (2 x 10 ml) and 0.1 N aqueous NaOH (2 x 10 ml). The organic phase was dried over Na_2SO_4, the solvent was removed, and the crude product was purified by flash chromatography (dichloromethane/MeOH = 1 to 10%) to give the product as a yellow amorphous solid. Yield: 61 mg, 0.22 mmol, 43%. ^{1}H NMR (500 MHz, DMSO-d_6) δ_H (ppm) = 13.42 (s, 1H), 10.72 (s, 1H), 10.54 (s, 1H), 7.89 (d, J = 2.0 Hz, 1H), 7.49 (s, 1H), 7.33 – 7.19 (m, 2H), 6.86 – 6.75 (m, 2H), 6.32 (dt, J = 3.7, 2.3 Hz, 1H), 4.02 (s, 1H). ^{13}C NMR (126 MHz, DMSO-d_6) δ_C (ppm) = 169.3, 149.4, 135.6, 132.2, 129.4, 126.0, 125.1, 125.1, 120.3, 119.0, 111.3, 110.7, 109.3, 75.9. MS (EI) m/z = 277 $[M]^+$. HPLC (254 nm): t_R = 4.639 min (95.7320%).

(*Z*)-*N*-(3-((1*H*-pyrrol-2-yl)methylene)-2-oxoindolin-5-yl)ethanesulfonamide (2h). To a solution of (*Z*)-3-((1*H*-pyrrol-2-yl)methylene)-5-aminoindolin-2-one (57 mg, 0.25 mmol, 1.0 equiv) in THF (5 ml) at 0°C was added diisopropyl ethyl amine (44 µl, 0.25 mmol, 1.0 equiv) and ethane sulfonyl chloride (24 µl, 0.25 mmol, 1.0 equiv). The solution was warmed to room temperature and stirred overnight. The reaction was quenched by the addition of brine (20 ml) and ethyl acetate (20 ml) and the organic layer was washed with saturated aqueous sodium bicarbonate solution (20 ml) and brine (20 ml) and dried with Na_2SO_4. The solvent was evaporated, and the crude product was purified by flash chromatography (dichloromethane/MeOH = 1 to 10%) to give the title compound as a yellow amorphous solid. Yield: 18 mg, 0.057 mmol, 23%. ^{1}H NMR (500 MHz, DMSO-d_6) δ_H (ppm) = 13.45 (s, 1H), 10.63 (s, 1H), 9.33 (s, 1H), 7.61 (ddd, J = 11.9, 8.2, 1.4 Hz, 1H), 7.41 (d, J = 2.0 Hz, 1H), 7.19 (dt, J = 3.8, 1.8 Hz, 1H), 7.01 (dd, J = 8.2, 2.1 Hz, 1H), 6.83 – 6.76 (m, 2H), 6.32 (dt, J = 3.7, 2.4

Hz, 1H), 2.99 (q, *J* = 7.4 Hz, 2H), 1.29 (t, *J* = 7.4 Hz, 3H). ^{13}C NMR (126 MHz, DMSO-d_6) δ_C (ppm) = 169.3, 136.1, 131.6, 131.4, 129.4, 128.3, 126.1, 124.9, 120.7, 120.2, 112.1, 111.3, 109.7, 44.5, 7.8. MS (EI) m/z = 317 $[M]^+$. HPLC (254 nm): t_R = 4.965 min (96.3844%).

(*Z*)-*N*-(3-((1*H*-pyrrol-2-yl)methylene)-2-oxoindolin-5-yl)ethenesulfonamide (2i). To a solution of (*Z*)-3-((1*H*-pyrrol-2-yl)methylene)-5-aminoindolin-2-one (112 mg, 0.5 mmol, 1.0 equiv) in THF (5 ml) was added diisopropyl ethyl amine (175 µl, 1.0 mmol, 2.0 equiv) and 2-chloroethane sulfonylchloride (53 µl, 0.5 mmol, 1.1 equiv). The reaction was stirred overnight at room temperature and quenched by the addition of brine (20 ml) and ethyl acetate (20 ml). The organic layer was dried over Na_2SO_4, the solvent was evaporated, and the crude product was purified by silica chromatography (dichloromethane/MeOH = 20/1) to give the title compound as a yellow amorphous solid. Yield: 57 mg, 0.18 mmol, 36%. ^{1}H NMR (500 MHz, DMSO-d_6) δ_H (ppm) = 13.42 (s, 1H), 10.69 (s, 1H), 7.51 (s, 1H), 7.37 (d, *J* = 2.0 Hz, 1H), 7.22 (td, *J* = 2.6, 1.4 Hz, 1H), 6.96 (dd, *J* = 8.2, 2.1 Hz, 1H), 6.83 (d, *J* = 1.9 Hz, 1H), 6.79 (d, *J* = 8.2 Hz, 1H), 6.32 (d, *J* = 3.7 Hz, 1H), 6.04 (d, *J* = 16.6 Hz, 1H), 5.90 (d, *J* = 10.0 Hz, 1H). ^{13}C NMR (126 MHz, DMSO-d_6) δ_C (ppm) = 169.3, 136.4, 136.0, 131.0, 129.5, 126.5, 126.3, 125.6, 125.1, 121.5, 120.4, 116.6, 113.0, 111.3, 109.6. MS (EI) m/z = 315 $[M]^+$. HPLC (254 nm): t_R = 5.227 min (96.8706%).

***N*-(3-((4-((5-Cyclopropyl-1*H*-pyrazol-3-yl)amino)pyrimidin-2-yl)amino)phenyl)acetamide (3a).** To a solution of N^2-(3-aminophenyl)-N^4-(5-cyclopropyl-1*H*-pyrazol-3-yl)pyrimidine-2,4-diamine (129 mg, 0.42 mmol, 1.0 equiv) in ethyl acetate (15 ml) at 0°C was added acetic anhydride (79.4 µl, 0.84 mmol, 2.0 equiv) and the mixture was stirred at room temperature overnight. The precipitate was isolated by filtration and dried under high vacuum to give the title compound as a yellow amorphous solid. Yield: 78 mg, 0.22 mmol, 52%. ^{1}H NMR

(500 MHz, DMSO-d_6) δ_H (ppm) = 11.99 (s, 1H), 9.83 (s, 1H), 9.44 (d, J = 85.0 Hz, 2H), 9.35 – 8.90 (m, 1H), 8.00 (d, J = 5.8 Hz, 1H), 7.95 – 7.72 (m, 1H), 7.59 – 7.38 (m, 1H), 7.30 – 6.94 (m, 2H), 6.38 (s, 1H), 2.06 (s, 3H), 1.86 (tt, J = 8.4, 5.0 Hz, 1H), 0.91 (dq, J = 6.4, 4.0 Hz, 2H), 0.80 – 0.63 (m, 2H). ^{13}C NMR (126 MHz, DMSO-d_6) δ_C (ppm) = 168.09, 159.54, 155.74, 141.09, 139.35, 128.34, 114.29, 112.32, 110.13, 98.25, 59.72, 23.98, 20.72, 14.06, 8.52, 7.63. MS (ESI): m/z = 350.18 $[M+H]^+$. HPLC (254 nm): t_R = 1.514 min (95.6875%).

***N*-(4-((4-((5-Cyclopropyl-1*H*-pyrazol-3-yl)amino)pyrimidin-2-yl)amino)phenyl)acetamid (3b).** To a solution of N^2-(4-aminophenyl)-N^4-(5-cyclopropyl-1*H*-pyrazol-3-yl)pyrimidine-2,4-diamine (200 mg, 0.651 mmol, 1.0 equiv) in dry THF (15 ml) at 0°C was added pyridine (58 µl, 0.716 mmol, 1.1 equiv) and acetic acid anhydride (68 µl, 0.716 mmol, 1.0 equiv) and the solution was stirred at room temperature overnight. The solvent was evaporated, and the crude product was purified by silica chromatography (dichloromethane/MeOH = 10/1) to give the title compound as a yellow amorphous solid. Yield: 124 mg, 0.355 mmol, 55%. ^{1}H NMR (500 MHz, DMSO-d_6) δ_H (ppm) = 12.05 (s, 1H), 9.78 (s, 1H), 9.57 (s, 1H), 9.05 (s, 1H), 7.97 (d, J = 5.7 Hz, 1H), 7.72 – 7.59 (m, 2H), 7.55 – 7.42 (m, 2H), 6.38 (s, 1H), 6.08 (s, 1H), 2.04 (s, 3H), 1.87 (tt, J = 8.4, 5.1 Hz, 1H), 0.98 – 0.82 (m, 2H), 0.76 – 0.59 (m, 2H). ^{13}C NMR (126 MHz, DMSO-d_6) δ_C (ppm) = 167.7, 159.6, 159.5, 155.9, 155.8, 136.2, 133.1, 119.3, 97.8, 59.7, 54.9, 23.8, 21.0, 20.7, 14.1, 7.7. MS (ESI): m/z = 350.18 $[M+H]^+$. HPLC (254 nm): t_R = 1.352 min (98.1651%).

2-Chloro-*N*-(3-((4-((5-cyclopropyl-1*H*-pyrazol-3-yl)amino)pyrimidin-2-yl)amino)phenyl)acet-amide (3c). To a stirred solution of N^2-(3-aminophenyl)-N^4-(5-cyclopropyl-1*H*-pyrazol-3-yl)pyrimidine-2,4-diamine (200 mg, 0.651 mmol, 1.0 equiv) in THF (5 ml) was added triethylamine (99 µl, 0.716 mmol, 1.1 equiv) and 2-chloroacetyl chloride (57 µl, 0.716 mmol,

1.1 equiv) in THF (2 ml). After one hour additional triethylamine (36 µl, 0.26 mmol, 0.4 equiv) and 2-chloroacetyl chloride (21µl, 0.26 mmol, 0.4 equiv) was added and the solution was stirred overnight. Saturated aqueous sodium hydrogen carbonate solution (15 ml) and brine (15 ml) were added and the mixture was extracted with ethyl acetate (40 ml). The organic layer was dried over Na_2SO_4, the solvent was removed, and the residue was purified by silica chromatography (dichloromethane/MeOH = 10/1) to give the title compound as a yellow amorphous solid. Yield: 100 mg, 0.261 mmol, 40%. ^{1}H NMR (500 MHz, DMSO-d_6) δ_H (ppm) = 11.97 (s, 1H), 10.21 (s, 1H), 9.48 (s, 1H), 9.09 (s, 1H), 7.93 (d, J = 71.4 Hz, 2H), 7.55 (d, J = 8.0 Hz, 1H), 7.23 (q, J = 11.5, 8.0 Hz, 2H), 6.38 (d, J = 67.1 Hz, 2H), 4.27 (s, 2H), 1.87 (tt, J = 8.5, 5.1 Hz, 1H), 0.92 (s, 2H), 0.78 – 0.58 (m, 2H). ^{13}C NMR (126 MHz, DMSO-d_6) δ_C (ppm) = 164.4, 159.5, 155.6, 148.2, 145.4, 141.3, 138.5, 128.5, 115.2, 112.5, 110.6, 98.4, 93.0, 43.6, 7.6, 6.9. MS (ESI): m/z = 384.14 $[M+H]^+$. HPLC (254 nm): t_R = 2.180 min (97.3103%).

2-Chloro-*N*-(4-((4-((5-cyclopropyl-1*H*-pyrazol-3-yl)amino)pyrimidin-2-yl)amino)phenyl)acet-amide (3d). To a stirred solution of N^2-(4-aminophenyl)-N^4-(5-cyclopropyl-1*H*-pyrazol-3-yl)pyrimidine-2,4-diamine (200 mg, 0.651 mmol, 1.0 equiv) in THF (15 ml) was added triethylamine (99 µl, 0.716 mmol, 1.1 equiv) and 2-chloroacetyl chloride (57 µl, 0.716 mmol, 1.1 equiv) and the solution was stirred overnight. Saturated aqueous sodium hydrogen carbonate solution (15 ml) and brine (15 ml) were added and the mixture was extracted with ethyl acetate (40 ml). The organic phase was dried with sodium sulfate, the solvent was removed, and the residue was purified by silica chromatography (dichloromethane/MeOH = 10/1) to give the title compound as a yellow amorphous solid. Yield: 95 mg, 0.248 mmol, 38%. ^{1}H NMR (500 MHz, DMSO-d_6) δ_H (ppm) = 12.00 (s, 1H), 10.18 (s, 1H), 9.49 (s, 1H), 9.04 (s, 1H), 8.11 – 7.85 (m, 1H), 7.70 (d, J = 8.6 Hz, 2H), 7.56 – 7.47 (m, 2H), 6.47 (d, J = 25.5 Hz,

1H), 6.33 – 6.11 (m, 1H), 4.24 (s, 2H), 1.87 (tt, *J* = 8.5, 5.1 Hz, 1H), 0.93 (d, *J* = 8.2 Hz, 2H), 0.69 (tt, *J* = 6.9, 4.4 Hz, 2H). ^{13}C NMR (126 MHz, DMSO-d_6) δ_C (ppm) = 164.0, 159.4, 155.6, 136.96, 132.0, 119.7, 97.9, 43.6, 7.7. MS (ESI): m/z = 384.14 $[M+H]^+$. HPLC (254 nm): t_R = 1.949 min (97.8748%).

***N*-(3-((4-((5-Cyclopropyl-1*H*-pyrazol-3-yl)amino)pyrimidin-2-yl)amino)phenyl)propionamide (3e).** To a solution of N^2-(3-aminophenyl)-N^4-(5-cyclopropyl-1*H*-pyrazol-3-yl)pyrimidine-2,4-diamine (200 mg, 0.651 mmol, 1.0 equiv) in dry THF (15 ml) was added pyridine (63 µl, 0.781 mmol, 1.2 equiv) and propionic acid anhydride (100 µl, 0.781 mmol, 1.2 equiv) and the solution was stirred at room temperature overnight. The solvent was evaporated, the residue was dissolved in ethyl acetate and washed with water (30 ml). The organic extract was dried over Na_2SO_4 and the solvent was removed. The crude product was purified by flash chromatography (dichloromethane/MeOH = 0 to 10%) to yield the product as a yellow amorphous solid. Yield: 111 mg, 0.305 mmol, 47%. ^{1}H NMR (500 MHz, DMSO-d_6) δ_H (ppm) = 11.97 (s, 1H), 9.76 (s, 1H), 9.49 (s, 1H), 9.04 (s, 1H), 8.00 (d, *J* = 5.6 Hz, 1H), 7.86 (s, 1H), 7.59 – 7.38 (m, 1H), 7.26 (d, *J* = 8.2 Hz, 1H), 7.17 (t, *J* = 8.0 Hz, 1H), 6.37 (s, 2H), 2.34 (q, *J* = 7.6 Hz, 2H), 1.86 (tt, *J* = 8.4, 5.0 Hz, 1H), 1.10 (t, *J* = 7.5 Hz, 3H), 0.91 (d, *J* = 8.1 Hz, 2H), 0.74 – 0.64 (m, 2H). ^{13}C NMR (126 MHz, DMSO-d_6) δ_C (ppm) = 171.8, 155.6, 141.1, 139.4, 128.3, 112.4, 98.2, 54.9, 40.0, 39.9, 39.7, 39.5, 39.4, 39.2, 39.0, 29.5, 9.7, 7.6. MS (ESI): m/z = 364.19 $[M+H]^+$. HPLC (254 nm): t_R = 1.922 min (96.0849%).

***N*-(4-((4-((5-Cyclopropyl-1*H*-pyrazol-3-yl)amino)pyrimidin-2-yl)amino)phenyl)propionamide (3f).** To a solution of N^2-(4-aminophenyl)-N^4-(5-cyclopropyl-1*H*-pyrazol-3-yl)pyrimidine-2,4-diamine (200 mg, 0.651 mmol, 1 equiv) in dry THF (15 ml) was added pyridine (58 µl, 0.716 mmol, 1.1 equiv) and propionic acid anhydride (91 µl, 0.716 mmol,

1.1 equiv) and the solution was stirred at room temperature overnight. The solvent was evaporated, and the residue was dissolved in ethyl acetate and washed with water (30 ml). The organic extract was dried over Na_2SO_4 and the solvent was removed. The crude product was purified by flash chromatography (dichloromethane/MeOH = 0 to 10%) to yield the product as a yellow amorphous solid. Yield: 104 mg, 0.286 mmol, 40%. ^{1}H NMR (500 MHz, DMSO-d_6) δ_H (ppm) = 12.17 (s, 1H), 10.00 (d, J = 15.7 Hz, 1H), 9.82 (s, 1H), 9.41 (s, 1H), 7.95 (d, J = 6.2 Hz, 1H), 7.57 (s, 4H), 6.42 (s, 1H), 6.05 (s, 1H), 2.33 (q, J = 7.6 Hz, 2H), 1.86 (tt, J = 8.4, 5.0 Hz, 1H), 1.11 (t, J = 7.6 Hz, 3H), 0.99 – 0.86 (m, 2H), 0.65 (dt, J = 6.6, 3.2 Hz, 2H). ^{13}C NMR (126 MHz, DMSO-d_6) δ_C (ppm) = 171.5, 159.5, 157.7, 134.4, 120.9, 119.3, 98.1, 51.4, 29.5, 28.7, 28.5, 28.4, 9.8, 7.7, 7.1. MS (ESI): m/z = 364.20 $[M+H]^+$. HPLC (254 nm): t_R = 1.674 min (95.2979%).

***N*-(3-((4-((5-Cyclopropyl-1*H*-pyrazol-3-yl)amino)pyrimidin-2-yl)amino)phenyl)acrylamide (3g).** To a stirred solution of N^2-(3-aminophenyl)-N^4-(5-cyclopropyl-1*H*-pyrazol-3-yl)pyrimidine-2,4-diamine (200 mg, 0.651 mmol, 1.0 equiv) in THF (15 ml) was added pyridine (58 µl, 0.716 mmol, 1.1 equiv) and acryloyl chloride (59 µl, 0.716 mmol, 1.1 equiv) and the solution was stirred for one hour at 0°C and at room temperature overnight. The solvent was evaporated, and the residue was taken up in ethyl acetate and washed with saturated aqueous sodium hydrogen carbonate solution (15 ml) and brine (15 ml). The organic layer was dried over Na_2SO_4, the solvent was removed, and the residue was purified by silica chromatography (dichloromethane/MeOH = 10/1) to give the title compound as a colorless amorphous solid. Yield: 62 mg, 0.171 mmol, 26%. ^{1}H NMR (500 MHz, DMSO-d_6) δ_H (ppm) = 11.97 (s, 1H), 10.06 (s, 1H), 9.46 (d, J = 68.4 Hz, 1H), 9.35 – 9.00 (m, 1H), 8.10 – 7.88 (m, 3H), 7.50 (dd, J = 8.2, 2.0 Hz, 1H), 7.37 (d, J = 8.2 Hz, 1H), 7.21 (t, J = 8.1 Hz, 1H), 6.50 (dd, J =

17.0, 10.2 Hz, 1H), 6.27 (dd, *J* = 16.9, 2.0 Hz, 1H), 5.75 (dd, *J* = 10.2, 2.1 Hz, 1H), 1.86 (tt, *J* = 8.4, 5.1 Hz, 1H), 0.90 (tt, *J* = 9.3, 5.4 Hz, 2H), 0.78 – 0.59 (m, 2H). ^{13}C NMR (126 MHz, DMSO-d_6) δ_C (ppm) = 163.0, 159.4, 141.1, 139.1, 132.1, 128.5, 126.5, 112.7, 98.3, 7.6. MS (ESI): m/z = 362.18 $[M+H]^+$. HPLC (254 nm): t_R = 1.933 min (95.0714%).

***N*-(4-((4-((5-Cyclopropyl-1*H*-pyrazol-3-yl)amino)pyrimidin-2-yl)amino)phenyl)acrylamide (3h).** To a stirred solution of N^2-(4-aminophenyl)-N^4-(5-cyclopropyl-1*H*-pyrazol-3-yl)pyrimidine-2,4-diamine (200 mg, 0.651 mmol, 1.0 equiv) in THF (15 ml) was added pyridine (58 µl, 0.716 mmol, 1.1 equiv) and acryloyl chloride (59 µl, 0.716 mmol, 1.1 equiv) and the solution was stirred for one hour at 0°C. The solvent was removed, and the residue was purified by silica chromatography (dichloromethane/MeOH = 10/1) to give the title compound as a colorless amorphous solid. Yield: 30 mg, 0.083 mmol, 13%. ^{1}H NMR (500 MHz, DMSO-d_6) δ_H (ppm) = 11.99 (s, 1H), 10.02 (s, 1H), 9.47 (s, 1H), 9.00 (s, 1H), 7.98 (d, *J* = 5.8 Hz, 1H), 7.70 (d, *J* = 8.6 Hz, 2H), 7.64 – 7.53 (m, 2H), 6.45 (dd, *J* = 16.9, 10.2 Hz, 1H), 6.25 (dd, *J* = 17.0, 2.1 Hz, 1H), 5.73 (dd, *J* = 10.2, 2.0 Hz, 1H), 1.87 (tt, *J* = 8.4, 5.0 Hz, 1H), 0.99 – 0.86 (m, 2H), 0.76 – 0.63 (m, 2H). ^{13}C NMR (126 MHz, DMSO-d_6) δ_C (ppm) = 162.6, 159.5, 155.9, 136.7, 132.6, 132.1, 126.1, 119.6, 119.3, 97.9, 14.1, 7.7. MS (ESI): m/z = 362.18 $[M+H]^+$. HPLC (254 nm): t_R = 1.703 min (96.9724%).

***N*-(3-((4-((5-Cyclopropyl-1*H*-pyrazol-3-yl)amino)pyrimidin-2-yl)amino)phenyl)propiolamide (3i).** To a stirred solution of N^2-(3-aminophenyl)-N^4-(5-cyclopropyl-1*H*-pyrazol-3-yl)pyrimidine-2,4-diamine (200 mg, 0.651 mmol, 1.0 equiv) in DMF (5 ml) at 0°C was added diisopropylethylamine (233 µl, 1.37 mmol, 2.1 equiv), propargylic acid (241 µl, 3.9 mmol, 6.0 equiv) and *N*-(3-dimethylaminopropyl)-*N*′-ethyl carbodiimide hydrochloride (263 mg, 1.37 mmol, 2.1 equiv) and the solution was stirred for two hours at 0°C.

The reaction mixture was diluted with ethyl acetate and the solvent was removed by freeze drying. The residue was purified by silica chromatography (dichloromethane/MeOH = 10/1) to give the title compound as a colorless amorphous solid. Yield: 12 mg, 0.033 mmol, 5%. ^{1}H NMR (500 MHz, DMSO-d_6) δ_H (ppm) = 11.99 (s, 1H), 9.47 (s, 1H), 9.05 (s, 1H), 7.97 (s, 2H), 7.70 (d, J = 8.6 Hz, 2H), 7.55 – 7.45 (m, 2H), 6.56 – 6.08 (m, 2H), 4.34 (s, 1H), 1.87 (tt, J = 8.5, 5.1 Hz, 1H), 0.93 (d, J = 8.1 Hz, 2H), 0.74 – 0.65 (m, 2H). ^{13}C NMR (126 MHz, DMSO-d_6) δ_C (ppm) = 159.9, 157.1, 153.5, 146.7, 135.0, 129.3, 117.6, 116.7, 116.7, 95.5, 76.2, 74.2, 5.3. MS (ESI): m/z = 360.15 $[M+H]^+$. HPLC (254 nm): t_R = 1.854 min (97.5080%).

***N*-(4-((4-((5-Cyclopropyl-1*H*-pyrazol-3-yl)amino)pyrimidin-2-yl)amino)phenyl)propiolamide (3j).** To a stirred solution of N^2-(4-aminophenyl)-N^4-(5-cyclopropyl-1*H*-pyrazol-3-yl)pyrimidine-2,4-diamine (130 mg, 0.42 mmol, 1.0 equiv) in DMF (10 ml) at 0°C was added diisopropylethylamine (150 µl, 0.882 mmol, 2.1 equiv), propargylic acid (150 µl, 2.52 mmol, 6.0 equiv) and *N*-(3-dimethylaminopropyl)-*N*′-ethyl carbodiimide hydrochloride (169 mg, 0.882 mmol, 2.1 equiv) and the solution was stirred for two hours at 0°C. The reaction mixture was diluted with ethyl acetate and washed with 0.1 N HCl (20 ml) and 0.1 N NaOH (20 ml) and the organic layer was dried with sodium sulfate and the solvent removed by freeze-drying. The residue was purified by silica chromatography (DCM/MeOH = 10/1) to give the title compound as a colorless amorphous solid. Yield: 26 mg, 0.072 mmol, 17%. ^{1}H NMR (500 MHz, DMSO-d_6) δ_H (ppm) = 11.97 (s, 1H), 10.71 (s, 1H), 9.49 (s, 1H), 9.06 (d, J = 39.8 Hz, 1H), 7.95 (d, J = 39.2 Hz, 2H), 7.56 (s, 1H), 7.21 (d, J = 5.1 Hz, 2H), 6.56 – 6.16 (m, 2H), 4.37 (s, 1H), 1.86 (tt, J = 8.4, 5.0 Hz, 1H), 0.96 – 0.85 (m, 2H), 0.74 – 0.64 (m, 2H). ^{13}C NMR (126 MHz, DMSO-d_6) δ_C (ppm) = 159.5, 155.5, 149.5, 141.2, 138.2, 128.5, 113.0, 98.3,

78.5, 76.8, 56.0, 18.5, 7.6. MS (ESI): m/z = 360.16 $[M+H]^+$. HPLC (254 nm): t_R = 1.692 min (99.0749%).

***N*-(3-((4-((5-Cyclopropyl-1*H*-pyrazol-3-yl)amino)pyrimidin-2-yl)amino)phenyl)ethanesulfon-amide (3k).** To a solution of N^2-(3-aminophenyl)-N^4-(5-cyclopropyl-1*H*-pyrazol-3-yl)pyrimidine-2,4-diamine (200 mg, 0.651 mmol, 1.0 equiv) in THF (10 ml) was added triethylamine (180 µl, 1.3 mmol, 2.0 equiv) and ethane sulfonyl chloride (123 µl, 1.3 mmol, 2.0 equiv) and the mixture was stirred at room temperature for 1 h and at 60°C for 1 h. The reaction mixture was cooled to room temperature, diluted with ethyl acetate and washed with brine and saturated aqueous sodium bicarbonate solution. The organic layer was dried over Na_2SO_4, the solvent was removed, and the residue was purified by silica chromatography (dichloromethane/MeOH = 10/1) to give the title compound as a yellow amorphous solid. Yield: 81 mg, 0.203 mmol, 31%. ^{1}H NMR (500 MHz, DMSO-d_6) δ_H (ppm) = 11.98 (s, 1H), 9.63 (s, 1H), 9.41 (s, 1H), 9.08 (s, 1H), 7.98 (s, 1H), 7.69 – 7.44 (m, 2H), 7.20 (t, J = 8.1 Hz, 1H), 6.86 – 6.74 (m, 1H), 6.46 (s, 1H), 6.30 (s, 1H), 3.12 (q, J = 7.3 Hz, 2H), 1.94 – 1.84 (m, 1H), 1.23 (t, J = 7.4 Hz, 3H), 0.98 – 0.85 (m, 2H), 0.71 (s, 2H). ^{13}C NMR (126 MHz, DMSO-d_6) δ_C (ppm) = 159.7, 159.5, 155.8, 148.1, 145.4, 141.8, 138.5, 128.9, 114.8, 112.4, 110.6, 98.4, 93.05, 54.9, 45.0, 7.99, 7.7, 6.8. MS (ESI): m/z = 400.16 $[M+H]^+$. HPLC (254 nm): t_R = 2.142 min (96.4205%).

***N*-(4-((4-((5-Cyclopropyl-1*H*-pyrazol-3-yl)amino)pyrimidin-2-yl)amino)phenyl)ethanesulfon-amide (3l).** To a solution of N^2-(4-aminophenyl)-N^4-(5-cyclopropyl-1*H*-pyrazol-3-yl)pyrimidine-2,4-diamine (200 mg, 0.651 mmol, 1.0 equiv) in THF (10 ml) was added triethylamine (180 µl, 1.3 mmol, 2.0 equiv) and ethane sulfonyl chloride (123 µl, 1.3 mmol, 2.0 equiv) and the mixture was stirred at room temperature for 1 h and at 60°C for

1 h. The reaction mixture was cooled to room temperature, diluted with ethyl acetate and washed with brine and saturated aqueous sodium bicarbonate solution. The organic layer was dried over Na_2SO_4, the solvent was removed, and the residue was purified by silica chromatography (dichloromethane/MeOH = 10/1) to give the title compound as a yellow amorphous solid. Yield: 102 mg, 0.256 mmol, 39%. ^{1}H NMR (500 MHz, DMSO-d_6) δ_H (ppm) = 11.99 (s, 1H), 9.46 (s, 2H), 9.02 (s, 1H), 8.13 – 7.91 (m, 1H), 7.71 (d, J = 8.3 Hz, 2H), 7.15 (d, J = 8.4 Hz, 2H), 6.49 (d, J = 39.7 Hz, 1H), 6.22 (s, 1H), 3.03 (q, J = 7.3 Hz, 2H), 1.88 (dq, J = 8.8, 5.0, 4.3 Hz, 1H), 1.23 (t, J = 7.3 Hz, 3H), 1.00 – 0.86 (m, 2H), 0.77 – 0.64 (m, 2H). ^{13}C NMR (126 MHz, DMSO-d_6) δ_C (ppm) = 159.5, 155.9, 148.1, 145.5, 137.7, 131.2, 121.3, 119.8, 98.0, 93.0, 54.9, 44.6, 8.0, 7.7, 6.8. MS (ESI): m/z = 400.16 $[M+H]^+$. HPLC (254 nm): t_R = 1.966 min (95.4217%).

***N*-(3-((4-((5-Cyclopropyl-1*H*-pyrazol-3-yl)amino)pyrimidin-2-yl)amino)phenyl)ethenesulfon-amide (3m).** To a stirred solution of N^2-(3-aminophenyl)-N^4-(5-cyclopropyl-1*H*-pyrazol-3-yl)pyrimidine-2,4-diamine (200 mg, 0.651 mmol, 1.0 equiv) in THF (10 ml) was added triethylamine (90 µl, 0.65 mmol, 1.0 equiv) and 2-chloroethanesulfonyl chloride (68 µl, 0.651 mmol, 1.0 equiv) and the solution was stirred for one hour at 0°C. Additional triethylamine (90 µl, 0.65 mmol, 1.0 equiv) was added and the mixture was stirred at room temperature overnight. The reaction mixture was diluted with ethyl acetate and washed with saturated aqueous sodium bicarbonate solution (15 ml) and brine (15 ml). The organic layer was dried over Na_2SO_4, the solvent was removed, and the residue was purified by flash chromatography (dichloromethane/MeOH = 100/1 to 10/1) to give the title compound as a yellow amorphous solid. Yield: 40 mg, 0.1 mmol, 15%. ^{1}H NMR (500 MHz, DMSO-d_6) δ_H (ppm) = 11.98 (s, 1H), 9.88 (d, J = 45.6 Hz, 1H), 9.50 (d, J = 85.1 Hz, 1H), 9.08 (s, 1H), 8.13 – 7.93 (m, 1H), 7.58 (d, J = 8.7 Hz, 2H), 7.16 (t, J = 7.7 Hz, 1H), 6.84 – 6.77 (m, 1H), 6.76 – 6.71

(m, 1H), 6.47 (s, 1H), 6.30 (s, 1H), 6.18 (d, J = 16.4 Hz, 1H), 6.06 (d, J = 9.9 Hz, 1H), 1.88 (s, 1H), 0.94 (d, J = 8.2 Hz, 2H), 0.70 (t, J = 13.8 Hz, 2H). ^{13}C NMR (126 MHz, DMSO-d_6) δ_C (ppm) = 161.0, 156.9, 149.4, 146.7, 143.0, 139.1, 137.6, 130.0, 128.8, 116.1, 113.7, 112.0, 99.8, 94.4, 56.2, 9.0, 8.1. MS (ESI): m/z = 398.15 $[M+H]^+$. HPLC (254 nm): t_R = 2.261 min (97.3760%).

***N*-(4-((4-((5-Cyclopropyl-1*H*-pyrazol-3-yl)amino)pyrimidin-2-yl)amino)phenyl)ethenesulfon-amide (3n).** To a stirred solution of N^2-(4-aminophenyl)-N^4-(5-cyclopropyl-1*H*-pyrazol-3-yl)pyrimidine-2,4-diamine (220 mg, 0.72 mmol, 1.0 equiv) in THF (10 ml) at 0°C was added triethylamine (119 µl, 0.86 mmol, 1.2 equiv) and 2-chloroethanesulfonyl chloride (90 µl, 0.86 mmol, 1.2 equiv) and the solution was stirred at room temperature overnight. Additional triethylamine (198 µl, 1.43 mmol, 2.0 equiv) and 2-chloroethanesulfonyl chloride (75 µl, 0.72 mmol, 1.0 equiv) were added and the mixture was stirred at room temperature overnight. The reaction mixture was diluted with ethyl acetate and washed with saturated aqueous sodium hydrogen carbonate solution (15 ml) and brine (15 ml). The organic phase was dried over Na_2SO_4, the solvent was removed, and the residue was purified by silica chromatography (dichloromethane/MeOH = 10/1) to give the title compound as a yellow amorphous solid. Yield: 24 mg, 0.06 mmol, 9%. ^{1}H NMR (500 MHz, CD_3OD) δ_H (ppm) = 7.82 (d, J = 6.0 Hz, 1H), 7.52 – 7.39 (m, 2H), 7.09 – 7.00 (m, 2H), 6.56 (dd, J = 16.5, 10.0 Hz, 1H), 6.17 (s, 1H), 6.02 (s, 1H), 5.83 (d, J = 9.9 Hz, 1H), 1.79 (tt, J = 8.5, 5.1 Hz, 1H), 0.91 – 0.76 (m, 2H), 0.61 (dq, J = 9.0, 3.4, 2.6 Hz, 2H). ^{13}C NMR (126 MHz, CD_3OD) δ_C (ppm) = 161.2, 156.9, 139.0, 137.2, 132.9, 127.7, 123.7, 123.0, 122.0, 117.4, 99.0, 8.3. MS (ESI): m/z = 398.15 $[M+H]^+$. HPLC (254 nm): t_R = 2.131 min (97.6470%).

(*Z*)-5-((5-(2-Chloroacetamido)-2-oxoindolin-3-ylidene)methyl)-*N*-(2-(diethylamino)ethyl)-2,4-dimethyl-1*H*-pyrrole-3-carboxamide (4a). To a solution of (*Z*)-5-((5-amino-2-oxoindolin-3-ylidene)methyl)-*N*-(2-(diethylamino)ethyl)-2,4-dimethyl-1*H*-pyrrole-3-carboxamide (37 mg, 0.093 mmol, 1.0 equiv) in dry THF (5 ml) at 0°C was added diisopropyl ethylamine (32 µl, 0.186 mmol, 2.0 equiv) and 2-chloro acetyl chloride (8.9 µl, 0.11 mmol, 1.2 equiv). The reaction mixture was stirred for 18 h and quenched with brine (30 ml) and ethyl acetate (30 ml) and extracted with ethyl acetate (2 x 30 ml). The organic layers were combined, dried over Na_2SO_4 and the solvent was evaporated. The crude product was purified by reversed-phase flash chromatography (acetonitrile/H_2O = 10 to 100%) to give the title compound as a yellow amorphous solid. Yield: 17 mg, 0.036 mmol, 39%. ^{1}H NMR (500 MHz, DMSO-d_6) δ_H (ppm) = 13.60 (s, 1H), 10.83 (s, 1H), 10.12 (s, 1H), 7.84 (s, 1H), 7.46 (s, 1H), 7.38 (t, J = 5.6 Hz, 1H), 7.23 (d, J = 8.5 Hz, 1H), 6.82 (d, J = 8.3 Hz, 1H), 4.21 (s, 2H), 2.55 – 2.43 (m, 8H), 2.41 (s, 3H), 2.37 (s, 3H), 0.95 (t, J = 7.1 Hz, 6H). ^{13}C NMR (126 MHz, DMSO-d_6) δ_C (ppm) = 169.5, 164.5, 164.3, 135.9, 135.1, 132.3, 129.3, 125.6, 125.6, 123.3, 119.0, 111.1, 109.4, 51.7, 46.5, 43.5, 37.0, 13.3, 11.8, 10.5. MS (ESI) m/z = 472.2 $[M+H]^+$. HPLC (254 nm): t_R = 2.872 min (100.0000%).

***(Z)*-*N*-(2-(Diethylamino)ethyl)-2,4-dimethyl-5-((2-oxo-5-(vinylsulfonamido)indolin-3-ylidene)-methyl)-1*H*-pyrrole-3-carboxamide (4b).** To a solution of (*Z*)-5-((5-amino-2-oxoindolin-3-ylidene)methyl)-*N*-(2-(diethylamino)ethyl)-2,4-dimethyl-1*H*-pyrrole-3-carboxamide (68 mg, 0.17 mmol, 1.0 equiv) in dry THF (10 ml) at 0°C was added triethylamine (46 µl, 0.34 mmol, 2.0 equiv) and 2-chloroethanesulfonyl chloride (36 µl, 0.34 mmol, 2.0 equiv). The reaction mixture was stirred for 18 h and quenched with brine (20 ml) and ethyl acetate (20 ml) and extracted with ethyl acetate (2 x 20 ml). The organic layers were combined,

dried over Na_2SO_4 and the solvent was evaporated. The crude product was purified by reversed-phase flash chromatography (acetonitrile/H_2O = 10 to 100%) to give the title compound as a yellow amorphous solid. Yield: 34 mg, 0.07 mmol, 41%. ^{1}H-NMR (500 MHz, $CDCl_3$ / DMSO-d_6 = 8/1) δ_H (ppm) = 13.35 (s, 1H), 10.02 (s, 1H), 7.08 (d, J = 2.0 Hz, 1H), 7.04 (s, 1H), 6.71 (dd, J = 8.3, 2.1 Hz, 1H), 6.51 (dd, J = 11.5, 7.0 Hz, 2H), 6.31 (dd, J = 16.6, 10.0 Hz, 1H), 5.83 (d, J = 16.7 Hz, 1H), 5.59 (d, J = 10.0 Hz, 1H), 3.23 – 3.18 (m, 2H), 2.45 (t, J = 6.1 Hz, 2H), 2.41 – 2.35 (m, 4H), 2.25 (s, 3H), 2.17 (s, 3H), 0.79 (d, J = 7.1 Hz, 6H). ^{13}C NMR (126 MHz, $CDCl_3$ / DMSO-d_6 = 8/1) δ_C (ppm) = 170.0, 165.5, 137.1, 136.20 135.6, 130.8, 128.9, 126.4, 126.3, 126.0, 123.0, 121.6, 119.2, 115.2, 113.2, 109.7, 51.4, 46.4, 36.5, 13.8, 11.3, 11.1. MS (ESI) m/z = 486.2 $[M+H]^+$. HPLC (254 nm): t_R = 2.862 min (96.1594%).

(*Z*)-5-((5-Acetamido-2-oxoindolin-3-ylidene)methyl)-*N*-(2-(diethylamino)ethyl)-2,4-dimethyl-1*H*-pyrrole-3-carboxamide (4c). To a solution of (*Z*)-5-((5-amino-2-oxoindolin-3-ylidene)methyl)-*N*-(2-(diethylamino)ethyl)-2,4-dimethyl-1*H*-pyrrole-3-carboxamide (71 mg, 0.18 mmol, 1.0 equiv) in dry THF (10 ml) at 0°C was added triethylamine (50 µl, 0.36 mmol, 2 eq.) and acetyl chloride (26 µl, 0.36 mmol, 2.0 equiv). The reaction mixture was stirred for 18 h at room temperature and then quenched with brine (30 ml) and ethyl acetate (30 ml) and extracted with ethyl acetate (2 x 30 ml). The organic layers were combined, dried over Na_2SO_4 and the solvent was evaporated. The crude product was purified by reversed-phase flash chromatography (acetonitrile/H_2O = 10 to 100%) to give the title compound as a yellow amorphous solid. Yield: 48 mg, 0.11 mmol, 61%. ^{1}H NMR (500 MHz, DMSO-d_6) δ_H (ppm) = 13.64 (s, 1H), 10.81 (s, 1H), 9.77 (s, 1H), 8.05 (t, *J* = 5.4 Hz, 1H), 7.83 (d, *J* = 2.1 Hz, 1H), 7.67 (s, 1H), 7.54 (t, *J* = 5.3 Hz, 1H), 7.44 (s, 1H), 7.27 (dd, *J* = 8.3, 2.0 Hz, 1H), 7.07 (d, *J* = 4.0 Hz, 1H), 6.83 (d, *J* = 8.3 Hz, 1H), 6.37 (d, *J* = 4.1 Hz, 1H), 6.28 (s, 1H), 3.30 – 3.25 (m, 1H), 3.12 (t,

J = 7.7 Hz, 2H), 2.48 (s, 3H), 2.46 (s, 3H), 2.40 (s, 3H), 2.26 (s, 3H), 2.04 (s, 3H). ^{13}C NMR (126 MHz, DMSO-d_6) δ_C (ppm) = 169.5, 167.8, 164.5, 135.7, 134.5, 133.3, 128.9, 125.5, 125.4, 122.8, 120.5, 118.7, 115.2, 110.7, 109.3, 51.7, 46.5, 37.0, 23.7, 13.3, 11.9, 10.4. . MS (ESI) m/z = 438.3 $[M+H]^+$. HPLC (254 nm): t_R = 1.823 min (95.7322%).

(*Z*)-*N*-(2-(Diethylamino)ethyl)-5-((5-(ethylsulfonamido)-2-oxoindolin-3-ylidene)methyl)-2,4-dimethyl-1H-pyrrole-3-carboxamide (4d). To a solution of (*Z*)-5-((5-amino-2-oxoindolin-3-ylidene)methyl)-*N*-(2-(diethylamino)ethyl)-2,4-dimethyl-1*H*-pyrrole-3-carboxamide (100 mg, 0.25 mmol, 1.0 equiv) in dry DMF (2 ml) was added pyridine (20 µl, 0.25 mmol, 1 eq.) and ethane sulfonyl chloride (24 µl, 0.25 mmol, 1.0 equiv). The reaction mixture was stirred for 18 h at room temperature and then quenched with brine (20 ml) and ethyl acetate (30 ml) and washed with brine (5 x 30 ml). The organic layer was dried over Na_2SO_4 and the solvent was evaporated. The crude product was purified by reversed-phase flash chromatography (acetonitrile/H_2O = 10 to 100%) to give the title compound as a yellow amorphous solid. Yield: 39 mg, 0. 08 mmol, 32 %. ^{1}H NMR (500 MHz, $CDCl_3$ / DMSO- d_6 = 8/1) δ_H (ppm) = 13.37 (s, 1H), 9.83 (s, 1H), 8.72 (s, 1H), 7.58 (t, J = 5.7 Hz, 1H), 7.22 (s, 1H), 7.12 (s, 1H), 6.92 (d, J = 8.1 Hz, 1H), 6.68 (d, J = 8.2 Hz, 1H), 3.69 (q, J = 5.7 Hz, 2H), 3.24 (t, J = 5.7 Hz, 2H), 3.12 (q, J = 7.4 Hz, 4H), 2.93 (t, J = 7.3 Hz, 2H), 2.35 (s, 3H), 2.28 (s, 3H), 1.33 – 1.17 (m, 9H). ^{13}C NMR (126 MHz, $CDCl_3$ / DMSO- d_6 = 8/1) δ_C (ppm) = 167.0, 141.4, 137.6, 136.0, 131.5, 129.8, 126.6, 126.2, 123.2, 120.9, 118.3, 115.4, 112.6, 110.0, 52.0, 48.0, 45.0, 35.3, 13.8, 10.9, 8.6, 8.0. MS (ESI) m/z = 488.24 $[M+H]^+$. HPLC (254 nm): t_R = 2.555 min (95.5186%).

(Z)-N-(2-(2-(4-(2,8-Diethyl-5,5-difluoro-1,3,7,9-tetramethyl-5*H*-4λ^4,5λ^4-dipyrrolo[1,2-c:2',1'-f][1,3,2]diazaborinin-10-yl)phenoxy)acetamido)ethyl)-2,4-dimethyl-5-((2-oxo-5-

(vinylsulfon-amido)indolin-3-ylidene)methyl)-1*H*-pyrrole-3-carboxamide (5a) To a solution of (*Z*)-*N*-(2-(2-(4-(2,8-diethyl-5,5-difluoro-1,3,7,9-tetramethyl-5*H*-4l4,5l4-dipyrrolo[1,2-c:2',1'-f][1,3,2]diazaborinin-10-yl)phenoxy)acetamido)ethyl)-2,4-dimethyl-5-((2-oxo-5-(2,2,2-trifluoro-acetamido)indolin-3-ylidene)methyl)-1*H*-pyrrole-3-carboxamide (56 mg, 0.064 mmol, 1.0 equiv) in water (6 ml) and MeOH (8 ml) was added potassium carbonate (25 mg, 0.179 mmol, 2.8 equiv) and the reaction mixture was stirred at room temperature for 18 h. Then, saturated sodium bicarbonate solution (20 ml) and dichloromethane (20 ml) were added, and the aqueous layer was extracted with dichloromethane (2 x 20 ml). The combined organic layers were washed with brine (3 x 50 ml), dried over $MgSO_4$ and filtered. The resulting solution was cooled to 0°C and 2-chloroethane sulfonyl chloride (10 µl, 0.1 mmol, 1.5 equiv) and triethylamine (18 µl, 0.13 mmol, 2.0 equiv) was added and the reaction mixture was stirred for 18 h at room temperature. The reaction was quenched with saturated aq. sodium bicarbonate solution (20 ml) and washed with brine (3 x 20 ml). The organic layer was dried over magnesium sulfate and the solvent was removed. The crude product was purified by silica chromatography (dichloromethane/MeOH = 20/1 to 10/1) to give the title compound as a red amorphous solid. Yield: 28 mg, 0.032 mmol, 51%. ^{1}H NMR (500 MHz, DMSO-d_6) δ_H (ppm) = 13.68 (s, 1H), 10.89 (s, 1H), 9.54 (s, 1H), 8.31 (dd, *J* = 11.6, 6.1 Hz, 1H), 7.71 (d, *J* = 5.3 Hz, 1H), 7.55 (d, *J* = 3.6 Hz, 2H), 7.29 (d, *J* = 8.5 Hz, 2H), 7.19 (d, *J* = 8.5 Hz, 2H), 6.96 (dd, *J* = 8.2, 2.0 Hz, 1H), 6.84 (d, *J* = 8.2 Hz, 1H), 6.78 (dd, *J* = 16.4, 10.0 Hz, 1H), 6.06 – 5.96 (m, 2H), 4.59 (s, 2H), 3.37 (s, 5H), 2.46 (s, 3H), 2.44 (s, 7H), 2.43 (s, 3H), 2.31 (q, *J* = 7.5 Hz, 5H), 1.32 (s, 6H), 0.95 (t, *J* = 7.5 Hz, 6H). ^{13}C NMR (126 MHz, DMSO-d_6) δ_C (ppm) = 169.5, 167.6, 165.1, 158.1, 153.0, 140.5, 138.1, 136.4, 136.1, 136.1, 136.0, 132.5, 130.9, 130.3, 129.8, 129.3, 127.4, 126.8, 126.0, 125.6, 123.7, 121.9, 120.5, 115.5, 114.7, 114.2, 109.6, 67.1, 38.7, 38.5, 16.4, 14.5, 13.3, 12.2,

11.5, 10.5. ^{11}B NMR (160 MHz, DMSO-d_6) δ_B (ppm) = 3.79 (t, J = 34.2 Hz) ppm. ^{19}F NMR (471 MHz, DMSO-d_6) δ_F (ppm) = -142.99 (dd, J = 66.5, 29.5 Hz) ppm. MS (APCI) m/z = 846.36 $[M-F]^+$. HPLC (360 nm): t_R = 8.685 min (95.2191%).

(*Z*)-5-((5-(2-Chloroacetamido)-2-oxoindolin-3-ylidene)methyl)-*N*-(2-(3-(5,5-difluoro-7,9-dimethyl-5*H*-4λ4,5λ4-dipyrrolo[1,2-c:2',1'-f][1,3,2]diazaborinin-3-yl)propanamido)ethyl)-2,4-dimethyl-1*H*-pyrrole-3-carboxamide (5b). To a solution of (*Z*)-*N*-(2-(3-(5,5-difluoro-7,9-dimethyl-5*H*-4λ^4,5λ^4-dipyrrolo[1,2-c:2',1'-f][1,3,2]diazaborinin-3-yl)propanamido)ethyl)-2,4-dimethyl-5-((2-oxo-5-(2,2,2-trifluoroacetamido)indolin-3-ylidene)methyl)-1*H*-pyrrole-3-carboxamide (26 mg, 0.037 mmol, 1.0 equiv) in water (7 ml) and MeOH (15 ml) was added potassium carbonate (10.2 mg, 0.074 mmol, 2.0 equiv) and the reaction mixture was stirred at room temperature for 18 h. Then, saturated aq. sodium bicarbonate solution (30 ml) and dichloromethane (30 ml) were added, and the aqueous layer was extracted with dichloromethane (2 x 30 ml). The combined organic extracts were washed with brine (3 x 50 ml), dried over $MgSO_4$ and filtered. The solution was cooled to 0°C and 2-chloro acetyl chloride (4.4 µl, 0.056 mmol, 1.5 equiv) and triethylamine (10.2 µl, 0.074 mmol, 2.0 equiv) was added and the reaction mixture was stirred for 18 h at room temperature. The reaction was quenched with saturated aq. sodium bicarbonate solution (20 ml) and washed with brine (3 x 20 ml). The organic layer was dried over magnesium sulfate and the solvent was removed. The crude product was purified by silica chromatography (dichloromethane/MeOH = 20/1) to give the title compound as a red amorphous solid. Yield: 7.6 mg, 0.011 mmol, 30%. ^{1}H NMR (500 MHz, DMSO-d_6) δ_H (ppm) = 13.65 (s, 1H), 10.87 (s, 1H), 10.14 (s, 1H), 8.06 (t, J = 5.5 Hz, 1H), 7.87 (d, J = 2.0 Hz, 1H), 7.66 (s, 1H), 7.55 (t, J = 5.4 Hz, 1H), 7.49 (s, 1H), 7.30 (dd, J = 8.3, 2.0 Hz, 1H), 7.06 (d, J = 4.0 Hz, 1H), 6.87 (d, J = 8.2 Hz, 1H), 6.37 (d, J = 4.0 Hz,

1H), 6.27 (s, 1H), 4.26 (s, 2H), 3.37 – 3.34 (m, 2H), 3.30 – 3.25 (m, 4H), 3.12 (t, *J* = 7.7 Hz, 2H), 2.48 (s, 3H), 2.46 (s, 3H), 2.41 (s, 3H), 2.26 (s, 3H). ^{13}C NMR (126 MHz, DMSO-d_6) δ_C (ppm) = 171.2, 169.5, 164.9, 164.3, 159.1, 157.7, 144.0, 136.1, 135.1, 134.4, 133.0, 132.3, 129.4, 128.8, 125.6, 125.2, 123.2, 120.4, 120.2, 118.9, 116.5, 114.9, 111.0, 109.4, 43.5, 38.8, 38.5, 33.8, 24.0, 14.5, 13.3, 10.9, 10.5. MS (ESI) m/z = 712.3 $[M+H]^+$. HPLC (360 nm): t_R = 5.183 min (96.1730%).

(*Z*)-*N*-(2-(2-(4-(2,8-Diethyl-5,5-difluoro-1,3,7,9-tetramethyl-5*H*-4λ^4,5λ^4-dipyrrolo[1,2-c:2',1'-f][1,3,2]diazaborinin-10-yl)phenoxy)acetamido)ethyl)-2,4-dimethyl-5-((2-oxo-5-(2,2,2-trifluoro-acetamido)indolin-3-ylidene)methyl)-1*H*-pyrrole-3-carboxamide

(5c) To a solution of 2-(4-(2,8-diethyl-5,5-difluoro-1,3,7,9-tetramethyl-5*H*-4λ^4,5λ^4-dipyrrolo[1,2-c:2',1'-f][1,3,2]-diazaborinin-10-yl)phenoxy)acetic acid (45 mg, 0.1 mmol, 1.0 equiv) in DMF was added 1-hydroxybenzotriazole hydrate (15 mg, 0.11 mmol, 1.1 equiv) and *N*-(3-dimethylaminopropyl)-*N*′-ethyl carbodiimide hydrochloride (20 mg, 0.1 mmol, 1.0 equiv) and the mixture was stirred for 30 min at room temperature. Then, a mixture of triethylamine (42 µl, 0.3 mmol, 3.0 equiv) and (*Z*)-*N*-(2-aminoethyl)-2,4-dimethyl-5-((2-oxo-5-(2,2,2-trifluoroacetamido)-indolin-3-ylidene)methyl)-1*H*-pyrrole-3-carboxamide hydrochloride (47 mg, 0.1 mmol, 1.0 equiv) was added and the reaction mixture was stirred for 18 h at room temperature. The reaction mixture was diluted with ethyl acetate (30 ml) and washed with 0.1 N hydrochloric acid, 0.1 N aq. sodium hydroxide solution and brine (each 3 x 30 ml). The combined organic extracts were dried over Na_2SO_4, the solvent was evaporated, and the crude product was purified by silica chromatography (dichloromethane/MeOH = 20/1) to give the title compound as a red amorphous solid. Yield: 56 mg, 0.064 mmol, 64%. ^{1}H NMR (500 MHz, DMSO-d_6) δ_H (ppm) = 13.65 (s, 1H), 11.12 (s, 1H), 10.96 (s, 1H), 8.30 (q, *J* = 7.5, 6.4 Hz, 1H),

7.95 (d, *J* = 2.0 Hz, 1H), 7.74 – 7.67 (m, 1H), 7.59 (s, 1H), 7.33 (dd, *J* = 8.3, 2.1 Hz, 1H), 7.32 – 7.24 (m, 2H), 7.22 – 7.15 (m, 2H), 6.93 (d, *J* = 8.3 Hz, 1H), 4.59 (s, 2H), 3.34 (s, 3H), 2.47 (s, 3H), 2.44 (d, *J* = 1.8 Hz, 8H), 2.30 (q, *J* = 7.4 Hz, 4H), 1.32 (s, 6H), 0.95 (t, *J* = 7.6 Hz, 6H). ^{13}C NMR (126 MHz, DMSO-d_6) δ_C (ppm) = 169.6, 167.6, 165.1, 158.1, 154.6, 152.9, 140.5, 138.1, 136.3, 132.5, 130.3, 129.9, 129.7, 129.3, 127.4, 125.8, 125.7, 123.8, 120.7, 120.5, 117.2, 115.5, 114.9, 114.6, 113.0, 109.5, 67.1, 38.7, 38.5, 16.4, 14.5, 13.3, 12.2, 11.5, 10.4. ^{11}B NMR (160 MHz, DMSO-d_6) δ_B (ppm) = 3.69 (t, *J* = 33.6 Hz). ^{19}F NMR (471 MHz, DMSO-d_6) δ_F (ppm) = -73.89, -143.02 (dd, *J* = 65.7, 28.2 Hz) ppm. MS (ESI) m/z = 852.37 $[M-F]^+$. HPLC (360 nm): t_R = 8.955 min (95.3825%).

(*Z*)-5-((5-(Acetamido)-2-oxoindolin-3-ylidene)methyl)-*N*-(2-(3-(5,5-difluoro-7,9-dimethyl-5*H*-4λ^4,5λ^4-dipyrrolo[1,2-c:2',1'-f][1,3,2]diazaborinin-3-yl)propanamido)ethyl)-2,4-dimethyl-1*H*-pyrrole-3-carboxamide (5d). To a solution of (*Z*)-*N*-(2-(3-(5,5-difluoro-7,9-dimethyl-5*H*-4λ^4,5λ^4-dipyrrolo[1,2-c:2',1'-f][1,3,2]diazaborinin-3-yl)propanamido)ethyl)-2,4-dimethyl-5-((2-oxo-5-(2,2,2-trifluoroacetamido)indolin-3-ylidene)methyl)-1*H*-pyrrole-3-carboxamide (15 mg, 0.021 mmol, 1.0 equiv) in water (5 ml) and MeOH (10 ml) was added potassium carbonate (5.8 mg, 0.042 mmol, 2.0 equiv) and the reaction mixture was stirred at room temperature for 18 h. Saturated aq. sodium bicarbonate solution (20 ml) and dichloromethane (20 ml) were added and the aqueous layer was extracted with dichloromethane (2 x 20 ml). The combined organic layers were washed with brine (3 x 50 ml), dried over $MgSO_4$ and filtered. The solution was cooled to 0°C and acetyl chloride (2.2 µl, 0.0315 mmol, 1.5 equiv) and triethylamine (5.8 µl, 0.042 mmol, 2.0 equiv) were added and the reaction mixture was stirred for 18 h at room temperature. The reaction was quenched with saturated sodium bicarbonate solution (20 ml) and washed with brine (3 x 20 ml). The organic layer was dried

over $MgSO_4$ and the solvent was removed. The crude product was purified by silica chromatography (dichloromethane/MeOH = 20/1) to give the title compound as a red amorphous solid. Yield: 6.5 mg, 0.01 mmol, 48 %. ^{1}H NMR (500 MHz, DMSO-d_6) δ_H (ppm) = 13.62 (s, 1H), 10.79 (s, 1H), 9.75 (s, 1H), 8.03 (t, J = 5.4 Hz, 1H), 7.81 (d, J = 2.1 Hz, 1H), 7.65 (s, 1H), 7.52 (t, J = 5.3 Hz, 1H), 7.42 (s, 1H), 7.25 (dd, J = 8.3, 2.0 Hz, 1H), 7.05 (d, J = 4.1 Hz, 1H), 6.81 (d, J = 8.4 Hz, 1H), 6.35 (d, J = 4.1 Hz, 1H), 6.26 (s, 1H), 3.26 (t, J = 5.5 Hz, 2H), 3.10 (t, J = 7.7 Hz, 2H), 2.46 (s, 3H), 2.43 (s, 3H), 2.38 (s, 3H), 2.24 (s, 3H), 2.02 (s, 3H). ^{13}C NMR (126 MHz, DMSO-d_6) δ_C (ppm) = 171.16, 169.51, 167.79, 164.88, 159.11, 157.69, 144.00, 135.90, 134.47, 133.27, 132.96, 129.14, 128.81, 125.53, 125.39, 125.21, 122.83, 120.21, 118.68, 116.47, 115.21, 110.70, 109.29, 38.79, 38.51, 33.76, 28.98, 23.95, 23.73, 14.47, 13.30, 10.94, 10.43. MS (ESI) m/z = 678.3 $[M+Na]^+$. HPLC (360 nm): t_R = 5.597 min (99.8730%).

Biology

Stock solutions of inhibitors

10 mM stock solutions of inhibitors in DMSO were made by dissolving 1 to 5 mg of solid in an appropriate amount of DMSO using an ultrasonic water bath (Compounds synthesized; Hypothemycin (Abcam); Sunitinib (LC Labs)) or were purchased as 10 mM DMSO Stock (Crenolanib, MedChemtronica).

Cell lines

Human Leukemia cell lines were purchased at DMSZ (MV4-11: ACC-102; THP-1 ACC-16; Jurkat: ACC-282) or provided by K. Stegmaier (NOMO1, U937, MOLM14). Cell lines were maintained in RPMI-1640 Medium supplemented with 10% FCS, 2 mM L-glutamine, penicillin

(100 U/ml) and streptomycin (100µg/ml) at 37°C at 5% CO_2. Cells were maintained at 0.25 to 1.5 x 10^6 Cells / ml.

Cell viability assays

Fluorescent Endpoint-Assay

For determining the effect of inhibitors on leukemia cell lines, cells were harvested at densities between 0.5 to 1.5 x 10^6 Cells / ml and subsequently seeded with 25.000 cells / well in a 96 well-plate in 90 µl of RPMI-1640 medium with 0.1% FCS. After 16 h, cells were treated with vehicle or different concentrations of inhibitor (10 µM, 1 µM, 500 nM, 100 nM, 50 nM, 10 nM, 5 nM, 1 nM) in triplicates and incubated at 37°C at 5% CO_2 for 72 h. Viable cells were quantified using the Celltiter Blue Assay (Promega) by adding 20 µl of Celltiter Blue reagent and incubation for 3 h at 37°C. Fluorescence was measured at a Tecan Infinite M1000 microplate reader (Exc. 530 nm, Em. 560 nm) and the relative inhibition of cell viability was calculated compared to vehicle control and cell-free control. Results were plotted to the logarithmic concentration of the inhibitor using Prism 7.02 (Graphpad San Diego, CA, USA) and the IC_{50} is determined using the equation "$Y=100/(1+10^{((LogIC50-X)*HillSlope)})$". Reported IC_{50} values are the mean values of two independent experiments (Figures S48 – S52).

Chemiluminescent Endpoint-Assay

For determining the effect of fluorescent inhibitors on leukemia cell lines, cells were harvested at densities between 0.5 to 1.5 x 10^6 Cells / ml and subsequently seeded with 10.000 cells / well in a 384 well-plate in 20 µl of RPMI-1640 medium with 0.1% FCS. After 16 h, cells were treated with vehicle or various concentrations of inhibitor (10 µM, 7.5 µM, 5 µM, 2.5 µM, 1 µM, 500 nM, 100 nM) in triplicates and incubated at 37°C at 5% CO_2 for 72 h.

Viable Cells were quantified using the Celltiter-Glo 2.0 Assay (Promega) by adding 20 µl of Celltiter-Glo reagent to each well at room temperature and cell lysis for 2 min using the shaking function of the Tecan M1000 reader. Luminescence was measured after 10 minutes using 500 ms integration time and the relative inhibition of cell viability was calculated compared to vehicle control and cell-free control. Results were plotted to the logarithmic concentration of the inhibitor using Prism 7.02 (Graphpad San Diego, CA, USA) and IC_{50} is determined using the equation "$Y=100/(1+10^{((LogIC50-X)*HillSlope)})$". For determination of cytotoxicity in U937, MOLM14 and NOMO1 cells, cells were resuspended at 15,000 cells/mL and seeded at 40 µl/ well onto 384-well plates. Cells were then treated with a single agent and analyzed for cell viability on day 0 and day 3 post-treatment using the Cell-TiterGlo luminescent assay kit (Promega) according to the manufacturer's protocol. Luminescence was read on a Fluostar Omega Reader (BMG Labtech).

Chemiluminescent RealTime-Glo MT Cell Viability Assay

For determining the time-dependent inhibition on FLT3-positive cells, MV4-11 cells were harvested at densities between 0.5 to 1.5 x 10^6 Cells / ml and subsequently seeded with 2.000 cells / well in a 384 well-plate in 27 µl of RPMI-1640 medium with 0.1% FCS. Cells were treated with vehicle or various concentrations of inhibitor (5 µM, 500 nM, 250 nM, 50 nM, 25 nM, 5 nM, 2.5 nM and 0.5 nM) in triplicates and incubated at 37°C at 5% CO_2 for 77 h (Figure S39). Viable Cells were quantified using the RealTime-Glo MT Cell Viability Assay (Promega) by adding 30 µl of 2-fold reagent mixture to each well. Cell viability was determined at 2 h, 4 h, 6 h, 8 h, 10 h, 12 h, 14 h, 16 h, 18 h, 20 h, 25 h, 27 h, 29 h, 31 h, 33 h, 35 h, 37 h, 49 h, 54 h, 57 h and 77 h measuring the luminescence using 500 ms integration time. The relative inhibition of cell viability was calculated compared to vehicle control and cell-free

control. Results were plotted to the logarithmic concentration of the inhibitor using Prism 7.02 (Graphpad San Diego, CA, USA) and IC_{50} is determined for each time-point indicated using the equation "$Y=100/(1+10^{((LogIC50-X)*HillSlope)})$".

Western Blot

Proteins were extracted using Lysis Buffer (Cell Signaling Technology) supplemented with Complete, EDTA-free Protease Inhibitor Cocktail (Roche Diagnostics). Protein samples were separated by SDS-PAGE and subsequently transferred to PVDF membranes, which were blocked in 5% BSA and incubated with primary antibodies against phospho FLT3 (Y969) (Cell Signaling Technology Cat. No. 3463), FLT3 (8F2) (Cell Signaling Technology Cat. No. 3462), phospho STAT5 (Y694) (Cell Signaling Technology Cat. No. 9351), STAT5 (Cell Signaling Technology Cat. No. 9363), GAPDH (Santa Cruz Biotechnology Cat. No. sc-47724). Membranes were washed in TBS-T and incubated with the appropriate horseradish peroxidase-conjugated secondary antibodies. Signal was detected by enhanced chemi-luminescence (ThermoFisher Scientific).

In-gel digest of FLT3 and MALDI-MS/MS analysis

2 µg of FLT3 *wt* diluted in 100 mM phosphate buffer (pH 7.4, total volume 100 µl) were incubated with 100 µM of compound for 5 h at 37°C. Samples were freeze-dried and denatured in 20 µl of 1x Lämmli buffer for 5 min at 95°C. Samples were purified by SDS gel electrophoresis (12% gel). Protein was stained using colloidal coomassie and the gel was destained using desalted water. Stained proteins in height of the 73 kDa marker were excised in 1 mm^3 cubes and washed alternatingly in 100 mM ammoniumbicarbonate buffer and acetonitrile (200 µl, 4 times each). 100 µl of 10 mM dithiothreitol in ammoniumbicarbonate buffer was added and incubated for 25 min at 60°C. The supernatant was discarded, and the gel pieces were

washed alternatingly in 100 mM ammoniumbicarbonate buffer and acetonitrile (4 times each). 100 µl of 10 mM iodoacetamide solution in ammoniumbicarbonate buffer were added and incubated at 37°C in the dark for 40 min. The supernatant was discarded, and the gel pieces were washed alternatingly in 100 mM ammoniumbicarbonate buffer and acetonitrile (4 times each). The gel pieces were rehydrated in 20 µl of 20 ng/µl Trypsin/Lys C mix (Promega) for 10 min, then covered with 60 µl 25 mM ammoniumbicarbonate buffer and incubated overnight. 10 µl of 1% formic acid was added and the supernatant was lyophilized. Samples were reconstituted in 10 µl of 0.1% trifluoro acetic acid and purified using µ-C18 ZipTip tips (Merck Millipore). Samples were spotted in a α-cyano-4-hydroxycinnamic acid matrix and spectra were recorded on a Bruker Daltonics autoFlex MALDI TOF spectrometer using positive polarity. Spectra were analyzed using Mmass 5.

Kinase inhibition assays

Determination of kinase inhibition was performed using the ADP Glo Assay (Promega) or determined by external services (Eurofins or DiscoverX) as indicated.

ADP Glo assay

The ADP Glo assay was used as described by the supplier. Active kinase was purchased from Promega (FLT3-D835Y, 50 ng per assay), Invitrogen (FLT3-ITD, 100 ng per assay) and ProQinase (FLT3-wt, 100 ng per assay). Kinase was mixed with 10-fold inhibitor and pre-incubated for the time indicated at each assay (5 to 30 min). Kinase Reaction Buffer A (4 µl) and a mixture (4 µl) of myelobasic protein (MBP, final concentration 0.1 mg/ml) and ATP (final concentration 100 µM to 1 mM) was added and the kinase reaction was incubated at room temperature for 120 min. ADP Glo reagent (10 µl) was added and incubated for 40 min at room temperature. Then, the kinase detection reagent (20 µl) was added and incubated for 30 min

(100 µM ATP) to 60 min (1 mM ATP) at room temperature. Relative Inhibition was calculated compared to vehicle control and reagent control and were plotted as relative inhibition of kinase activity to the logarithmic concentration of the inhibitor using Prism 7.02 (Graphpad, San Diego, CA, USA). IC_{50} is determined using the equation "$Y=100/(1+10^{((LogIC50-X)*HillSlope)})$". K_i and k_{inact} of compounds **4a** and **4b** have been determined using the ADP Glo assay with pre-incubation times of 2 min, 10 min, 20 min and 30 min. The time-dependent IC_{50} values were fitted to the following equation using nonlinear regression:

$$y=(((1+(S/K_M))*K_I)/(((k_{inact}*(y/((K_I*(1+(S/K_M)))+y)))*x)/((2-((k_{inact}*(y/((K_I*(1+(S/K_M)))+y)))*x))-(2*exp((((-1)*k_{inact})*(y/((K_I*(1+(S/K_M)))+y)))*x)))))$$

where K_I and k_{inact} can be calculated as reported by Krippendorf et al.[42] using GraphPad Prism 8.0.1.

Kinase Screening at Eurofins Pharma Drug Discovery Series and DiscoverX

K_d measurements for **4b** were performed using the KINOMEscan® Assay Platform (DiscoverX, San Diego, United States). Assays were run using an 11-point 3-fold dilutional series starting at 30 µM inhibitor. Single-point determination of residual kinase activity for **4b** was performed using the KinaseProfiler platform (Eurofins, Dundee, United Kingdom). Assays were run using 10 µM ATP and kinase activity was measured by scintillation. Relative inhibition was calculated compared to vehicle control and reagent control. Kinase tree was illustrated using KinMap.[36]

Zebrafish Maintenance and Husbandry

Adult zebrafish wildtype (*Danio rerio*) are maintained in 60 l fish tanks in a laboratory with no daylight and a constant temperature of 28°C. Room light is programmed to a 12 h dark / 12 h light cycle. Adult zebrafish are bred in mating containers (2 animals / 1 l) or mating tanks (6 – 8

animals / 20 l) that are equipped with plastic grass and a removable sieve at the bottom of the tank. Embryos are collected 2 to 3 hours after a light cycle started, rinsed with E3-Medium and isolated in petri dishes containing E3-Medium. Living embryos were sorted randomly 24 hours past fertilization in 96 well plates (n=1 / Well) or 24 Well plate (n = 10 / Well). Fish keeping protocols are approved by the Darmstadt administrative authority and documented. All fish were treated humanely.

Danio rerio Toxicity Assay

Stock solutions (10 mM in DMSO) of test compounds are diluted to 10x final concentrations. Embryos are sorted in 180 µl of E3 Medium and 24 hpf test compounds are added to give the final 1x concentrations. Survival was monitored every 24 h by observation of heart-beat. Embryos were euthanized 120 h past fertilization using eugenol. Survival rates were calculated compared to 0.1 % DMSO-treated controls and fish water controls. Images were recorded using a Panasonic Lumix GX8 equipped with a Lumix G macro 1:2.8/30 ASPH objective and a 10 mm and 16 mm extension tube (Meike MK-P-AF3B). Fluorescence was recorded using an AxioScopeA.1 microscope (Zeiss) equipped with an Axiocam MRc or equipped with a Nuance FX multispectral imaging system.

Determination of compound half-life time

Inhibitor half-life has been determined using 1.5 ml HPLC vials injecting 20 µl per run using the HPLC method as described above. All buffers are sonicated for 30 min in an open flask and have been purged with argon for 6 hours. 5 µl of a 1 mM DMSO Stock solution of inhibitor was mixed with 45 µl of acetonitrile, 50 µl of a 10 mM solution of nucleophile in 100 mM potassium phosphate buffer at the pH value indicated and 400 µl of 100 mM potassium phosphate buffer under argon immediately before the first injection into the HPLC. The samples have been

measured at t = 0 min, 34 min, 68 min, 102 min, 136 min, 170 min, 204 min. The area of the signal corresponding to the inhibitor was determined (mAU·s) and the relative area compared to the first measurement was plotted to the corresponding time-point. The half-life was determined using one-phase exponential decay fit of Graphpad Prism 7.02 ($Y = (Y_0 - \text{Plateau}) \cdot \exp^{(-K*X)} + \text{Plateau}$). Half-life is calculated as $t_{1/2} = \ln(2) / k$.

Detection of fluorescence using SDS-PAGE and subsequent Western blotting

500 ng FLT3-D835Y (Promega, 10 µl) is diluted in 100 mM phosphate buffer (pH 7.4, total volume 100 µl) and is incubated with 100 µM of compound for 3 h at 37°C. Then 1 µl of 100-fold DMSO stock of the fluorophore is added (final concentration 1 µM) and incubated for 2 h at 37°C. Samples were freeze-dried and reconstituted with 10 µl of a 10 mM solution of GSH and incubated for 2 h at 37°C. Then the samples are denatured by adding 10 µl of 2x Lämmli buffer and incubation for 5 min at 95°C. Samples are subjected to SDS gel electrophoresis (12% gel) and subsequently blotted to a PVDF membrane using constant ampere (2 mA / cm^2 gel, 45 min) and Western blot buffer (48 mM Tris, 39 mM glycine, 10% methanol). The blotting membrane was washed with water twice and dried in an air flow for 30 min. Fluorescence was recorded using a Vilber Fusion FX7 Edge imaging system using the settings indicated in the corresponding image.

ASSOCIATED CONTENT

Supporting Information. Supporting Figures S1-S52 and Supporting Tables S1-S9. Synthesis and compound characterization data of synthesis intermediates, NMR spectra of test compounds,

dose-response curves, molecular formula strings of compounds. This material is available free of charge via the Internet at http://pubs.acs.org.

AUTHOR INFORMATION

Corresponding Author

* schmidt_boris@mac.com

Author Contributions

The manuscript was written through contributions of all authors. All authors have given approval to the final version of the manuscript.

Funding Sources

This work was supported by the Leukemia & Lymphoma Society (K.St.) and the National Cancer Institute R35 CA210030-01 (K.St.).

Notes

K.St. participates in the DFCI/Novartis Drug Discovery Program which includes grant support for an unrelated project and previously included consulting and has consulted for Rigel Pharmaceuticals on a topic unrelated to this manuscript.

ACKNOWLEDGMENT

The authors thank Dr. Tobias Meckel and Anke Imrich for technical assistance; Dr. Christoph Scholz for helpful discussions, and Merck Lab for access to the Vilber Imaging system.

Authors will release the atomic coordinates and experimental data upon article publication.

ABBREVIATIONS

FLT3, FMS-like tyrosine kinase 3; ITD, internal tandem duplications; TKI, tyrosine kinase inhibitor; CRG, chemical reactive group; HA, α-halo acetamide; AC, acrylamide; VS, vinyl sulfonamide; PA, propargyl amide; HY, hypothemycin; SU, sunitinib.

REFERENCES

1. De Kouchkovsky, I.; Abdul-Hay, M., 'Acute myeloid leukemia: a comprehensive review and 2016 update'. *Blood Cancer J* **2016,** *6*, e441.

2. Smith, C. C.; Wang, Q.; Chin, C. S.; Salerno, S.; Damon, L. E.; Levis, M. J.; Perl, A. E.; Travers, K. J.; Wang, S.; Hunt, J. P.; Zarrinkar, P. P.; Schadt, E. E.; Kasarskis, A.; Kuriyan, J.; Shah, N. P., Validation of ITD mutations in FLT3 as a therapeutic target in human acute myeloid leukaemia. *Nature* **2012,** *485* (7397), 260-263.

3. Smith, C. C.; Lin, K.; Stecula, A.; Sali, A.; Shah, N. P., FLT3 D835 mutations confer differential resistance to type II FLT3 inhibitors. *Leukemia* **2015,** *29*, 2390-2392.

4. Stone, R. M.; Manley, P. W.; Larson, R. A.; Capdeville, R., Midostaurin: its odyssey from discovery to approval for treating acute myeloid leukemia and advanced systemic mastocytosis. *Blood Adv.* **2018,** *2* (4), 444-453.

5. Barf, T.; Kaptein, A., Irreversible protein kinase inhibitors: balancing the benefits and risks. *J. Med. Chem.* **2012,** *55* (14), 6243-6262.

6. Dungo, R. T.; Keating, G. M., Afatinib: First global approval. *Drugs* **2013,** *73* (13), 1503-1515.

7. Neratinib approved for HER2+ Breast Cancer. *Cancer discovery* **2017,** *7* (9), Of1.

8. Greig, S. L., Osimertinib: first global approval. *Drugs* **2016,** *76* (2), 263-273.

9. de Claro, R. A.; McGinn, K. M.; Verdun, N.; Lee, S.-L.; Chiu, H.-J.; Saber, H.; Brower, M. E.; Chang, C. J. G.; Pfuma, E.; Habtemariam, B.; Bullock, J.; Wang, Y.; Nie, L.; Chen, X.-H.; Lu, D.; Al-Hakim, A.; Kane, R. C.; Kaminskas, E.; Justice, R.; Farrell, A. T.; Pazdur, R., FDA approval: Ibrutinib for patients with previously preated mantle cell lymphoma and previously treated chronic lymphocytic leukemia. *Clin. Cancer Res.* **2015,** *21* (16), 3586-3590.

10. Schirmer, A.; Kennedy, J.; Murli, S.; Reid, R.; Santi, D. V., Targeted covalent inactivation of protein kinases by resorcylic acid lactone polyketides. *Proc. of the Nat. Acad. Sci. U. S. A.* **2006,** *103* (11), 4234-4239.

11. Chaikuad, A.; Koch, P.; Laufer, S. A.; Knapp, S., The cysteinome of protein kinases as a target in drug development. *Angew. Chem. Int. Ed.* **2018,** *57* (16), 4372-4385.

12. Rastelli, G.; Rosenfeld, R.; Reid, R.; Santi, D. V., Molecular modeling and crystal structure of ERK2–hypothemycin complexes. *J. Struct. Biol.* **2008,** *164* (1), 18-23.

13. Wissner, A.; Floyd, M. B.; Johnson, B. D.; Fraser, H.; Ingalls, C.; Nittoli, T.; Dushin, R. G.; Discafani, C.; Nilakantan, R.; Marini, J.; Ravi, M.; Cheung, K.; Tan, X.; Musto, S.; Annable, T.; Siegel, M. M.; Loganzo, F., 2-(Quinazolin-4-ylamino)-[1,4]benzoquinones as covalent-

binding, rrreversible rnhibitors of the kinase domain of vascular endothelial growth factor receptor-2. *J. Med. Chem.* **2005,** *48* (24), 7560-7581.

14. Xu, J.; Ong, E. H. Q.; Hill, J.; Chen, A.; Chai, C. L. L., Design, synthesis and biological evaluation of FLT3 covalent inhibitors with a resorcylic acid core. *Biorg. Med. Chem.* **2014,** *22* (23), 6625-6637.

15. Scarpino, A.; Ferenczy, G. G.; Keserű, G. M., Comparative evaluation of covalent docking tools. *J. Chem. Inf. Model.* **2018,** *58* (7), 1441-1458.

16. Scholz, C.; Knorr, S.; Hamacher, K.; Schmidt, B., DOCKTITE—A highly versatile step-by-step workflow for covalent docking and virtual screening in the Molecular Operating Environment. *J. Chem. Inf. Model.* **2015,** *55* (2), 398-406.

17. *Molecular Operating Environment (MOE), 2013.08; Chemical Computing Group ULC, 1010 Sherbooke St. West, Suite #910, Montreal, QC, Canada, H3A 2R7, 2018.*

18. Latorre, A.; Schirmeister, T.; Kesselring, J.; Jung, S.; Johé, P.; Hellmich, U. A.; Heilos, A.; Engels, B.; Krauth-Siegel, R. L.; Dirdjaja, N.; Bou-Iserte, L.; Rodríguez, S.; González, F. V., Dipeptidyl nitroalkenes as potent reversible inhibitors of cysteine proteases rhodesain and cruzain. *ACS Med. Chem. Lett.* **2016,** *7* (12), 1073-1076.

19. Schirmeister, T.; Schmitz, J.; Jung, S.; Schmenger, T.; Krauth-Siegel, R. L.; Gütschow, M., Evaluation of dipeptide nitriles as inhibitors of rhodesain, a major cysteine protease of Trypanosoma brucei. *Bioorg. Med. Chem. Lett.* **2017,** *27* (1), 45-50.

20. Royo, S.; Schirmeister, T.; Kaiser, M.; Jung, S.; Rodríguez, S.; Bautista, J. M.; González, F. V., Antiprotozoal and cysteine proteases inhibitory activity of dipeptidyl enoates. *Biorg. Med. Chem.* **2018,** *26* (16), 4624-4634.

21. LaMonte, G. M.; Almaliti, J.; Bibo-Verdugo, B.; Keller, L.; Zou, B. Y.; Yang, J.; Antonova-Koch, Y.; Orjuela-Sanchez, P.; Boyle, C. A.; Vigil, E.; Wang, L.; Goldgof, G. M.; Gerwick, L.; O'Donoghue, A. J.; Winzeler, E. A.; Gerwick, W. H.; Ottilie, S., Development of a potent inhibitor of the plasmodium proteasome with reduced mammalian toxicity. *J. Med. Chem.* **2017,** *60* (15), 6721-6732.

22. London, N.; Miller, R. M.; Krishnan, S.; Uchida, K.; Irwin, J. J.; Eidam, O.; Gibold, L.; Cimermančič, P.; Bonnet, R.; Shoichet, B. K.; Taunton, J., Covalent docking of large libraries for the discovery of chemical probes. *Nature Chem. Biol.* **2014,** *10*, 1066-1072.

23. Shraga, A.; Olshvang, E.; Davidzohn, N.; Khoshkenar, P.; Germain, N.; Shurrush, K.; Carvalho, S.; Avram, L.; Albeck, S.; Unger, T.; Lefker, B.; Subramanyam, C.; Hudkins, R. L.; Mitchell, A.; Shulman, Z.; Kinoshita, T.; London, N., Covalent docking identifies a potent and selective MKK7 Inhibitor. *Cell chem biol* **2019,** *26* (1), 98-108.e5.

24. Mol, C. D.; Lim, K. B.; Sridhar, V.; Zou, H.; Chien, E. Y. T.; Sang, B.-C.; Nowakowski, J.; Kassel, D. B.; Cronin, C. N.; McRee, D. E., Structure of a c-Kit product complex reveals the basis for kinase transactivation. *J. Biol. Chem.* **2003,** *278* (34), 31461-31464.

25. Larrosa-Garcia, M.; Baer, M. R., FLT3 Inhibitors in acute myeloid leukemia: current status and future directions. *Mol. Cancer Ther.* **2017,** *16* (6), 991-1001.

26. Liu, T.; Lin, Y.; Wen, X.; Jorissen, R. N.; Gilson, M. K., BindingDB: a web-accessible database of experimentally determined protein–ligand binding affinities. *Nucleic Acids Res.* **2007,** *35* (suppl_1), D198-D201.

27. Liao, J. J.-L., Molecular recognition of protein kinase binding pockets for design of potent and selective kinase inhibitors. *J. Med. Chem.* **2007,** *50* (3), 409-424.

28. Neudert, G.; Klebe, G., DSX: A knowledge-based scoring function for the assessment of protein–ligand complexes. *J. of Chem. Inf. Model.* **2011,** *51* (10), 2731-2745.

29. Statsuk, A. V.; Maly, D. J.; Seeliger, M. A.; Fabian, M. A.; Biggs, W. H.; Lockhart, D. J.; Zarrinkar, P. P.; Kuriyan, J.; Shokat, K. M., Tuning a three-component reaction for trapping kinase substrate complexes. *J. Am. Chem. Soc.* **2008,** *130* (51), 17568-17574.

30. Zhao, Q.; Ouyang, X.; Wan, X.; Gajiwala, K. S.; Kath, J. C.; Jones, L. H.; Burlingame, A. L.; Taunton, J., Broad-spectrum kinase profiling in live cells with lysine-targeted sulfonyl fluoride probes. *J. Am. Chem. Soc.* **2017,** *139* (2), 680-685.

31. Braunbeck, T.; Kais, B.; Lammer, E.; Otte, J.; Schneider, K.; Stengel, D.; Strecker, R., The fish embryo test (FET): origin, applications, and future. *Environ. Sci. Pollut. Res.* **2015,** *22* (21), 16247-16261.

32. Fabian, M. A.; Biggs, W. H., 3rd; Treiber, D. K.; Atteridge, C. E.; Azimioara, M. D.; Benedetti, M. G.; Carter, T. A.; Ciceri, P.; Edeen, P. T.; Floyd, M.; Ford, J. M.; Galvin, M.; Gerlach, J. L.; Grotzfeld, R. M.; Herrgard, S.; Insko, D. E.; Insko, M. A.; Lai, A. G.; Lelias, J. M.; Mehta, S. A.; Milanov, Z. V.; Velasco, A. M.; Wodicka, L. M.; Patel, H. K.; Zarrinkar, P. P.;

Lockhart, D. J., A small molecule-kinase interaction map for clinical kinase inhibitors. *Nat. Biotechnol.* **2005,** *23* (3), 329-336.

33. Mologni, L.; Rostagno, R.; Brussolo, S.; Knowles, P. P.; Kjaer, S.; Murray-Rust, J.; Rosso, E.; Zambon, A.; Scapozza, L.; McDonald, N. Q.; Lucchini, V.; Gambacorti-Passerini, C., Synthesis, structure–activity relationship and crystallographic studies of 3-substituted indolin-2-one RET inhibitors. *Biorg. Med. Chem.* **2010,** *18* (4), 1482-1496.

34. Zimmerman, E. I.; Turner, D. C.; Buaboonnam, J.; Hu, S.; Orwick, S.; Roberts, M. S.; Janke, L. J.; Ramachandran, A.; Stewart, C. F.; Inaba, H.; Baker, S. D., Crenolanib is active against models of drug-resistant FLT3-ITD−positive acute myeloid leukemia. *Blood* **2013,** *122* (22), 3607-3615.

35. Davis, M. I.; Hunt, J. P.; Herrgard, S.; Ciceri, P.; Wodicka, L. M.; Pallares, G.; Hocker, M.; Treiber, D. K.; Zarrinkar, P. P., Comprehensive analysis of kinase inhibitor selectivity. *Nat. Biotechnol.* **2011,** *29*, 1046-1051.

36. Eid, S.; Turk, S.; Volkamer, A.; Rippmann, F.; Fulle, S., KinMap: a web-based tool for interactive navigation through human kinome data. *BMC Bioinformatics* **2017,** *18* (1), 16.

37. Wodicka, L. M.; Ciceri, P.; Davis, M. I.; Hunt, J. P.; Floyd, M.; Salerno, S.; Hua, X. H.; Ford, J. M.; Armstrong, R. C.; Zarrinkar, P. P.; Treiber, D. K., Activation state-dependent binding of small molecule kinase inhibitors: structural insights from biochemistry. *Chem. Biol.* **2010,** *17* (11), 1241-1249.

38. Turetsky, A.; Kim, E.; Kohler, R. H.; Miller, M. A.; Weissleder, R., Single cell imaging of brutons tyrosine kinase using an irreversible inhibitor. *Sci. Rep.* **2014,** *4*, 4782.

39. Sturgeon, J. B.; Laird, B. B., Symplectic algorithm for constant-pressure molecular dynamics using a Nosé–Poincaré thermostat. *J. Chem. Phys.* **2000,** *112* (8), 3474-3482.

40. Amombo, G. M.; Kramer, T.; Lo Monte, F.; Goring, S.; Fach, M.; Smith, S.; Kolb, S.; Schubenel, R.; Baumann, K.; Schmidt, B., Modification of a promiscuous inhibitor shifts the inhibition from gamma-secretase to FLT-3. *Bioorg Med Chem Lett* **2012,** *22* (24), 7634-7640.

41. Fu, H. Y.; Chen, L.; Doucet, H., Phosphine-free palladium-catalyzed direct arylation of imidazo[1,2-a]pyridines with aryl bromides at low catalyst loading. *J. Org. Chem.* **2012,** *77* (9), 4473-4478.

42. Krippendorff, B. F.; Neuhaus, R.; Lienau, P.; Reichel, A.; Huisinga, W., Mechanism-based inhibition: deriving K(I) and k(inact) directly from time-dependent IC(50) values. *J. biomol. screen.* **2009,** *14* (8), 913-923.

Table of Contents graphic